Transport in Porous Media (2026) 153:71
https://doi.org/10.1007/s11242-026-02321-5

Modified Theoretical Model for Temperature-Dependent Electro-Kinetic Properties of Porous Media

P. W. J. Glover[1]

Received: 18 December 2025 / Accepted: 13 May 2026 / Published online: 4 June 2026

Abstract
I report theoretical modelling of streaming potential coefficient C_{sp} and zeta potential ζ in porous media with NaCl electrolytes as a function of temperature up to 150°C. The modelling captures the essential behaviour of both C_{sp} and ζ as a function of both temperature, salinity and pH, the latter of which also depends on temperature and salinity. The modelling also shows ζ which is negative, decreasing in magnitude with temperature, and as pH becomes smaller. It also shows that C_{sp} is also negative but has a complex temperature and pH dependence. These behaviours are controlled mainly by the temperature dependence of pH, but also depend on the temperature dependence of the density, viscosity, relative permittivity and electrical conductivity of the pore solution. The model has been compared to experimental data for sandstones up to 150°C, and describes the data reasonably well when using physically reasonable values for the electro-chemical parameters describing the electrical double layer. This modelling has implications for the calculation of electro-kinetic parameters in geothermal reservoirs, CCUS targets and radioactive storage underground.

keywords zeta potential · streaming potential · porous material · temperature · pH · uid salinity

1 Introduction

The temperature dependence of the steady-state streaming potential coefficient C_{sp} and zeta potential ζ of rock samples are important because their magnitude and frequency-dependence (Tardif et al. 2011, 2012; Glover 2018; Glover et al. 2012a, b, 2020; Walker and Glover 2018) determine the size of coupling between fluid and electrical flow in techniques such as electro-seismics (Saunders et al. 2008; Dupuis et al. 2009). Applications of these electro-kinetic parameters are found in hydrocarbon, geothermal resources, aquifers and prospective sites for carbon capture and storage by deep underground injection, and the storage of radioactive waste in the subsurface. All these applications involve elevated temperatures.

✉ P. W. J. Glover
p.w.j.glover@leeds.ac.uk

[1] School of Earth, Environment and Sustainability, University of Leeds, Leeds, UK

However, it is not clear whether C_{sp} and of rock samples increases or decreases with temperature. Previous measurement and modelling have focussed on the variation of C_{sp} and ζ with pH, frequency and microstructure (Walker et al. 2014; Glover 2018; Walker and Glover 2018; Peng et al. 2020). Vinogradov and Jackson (2015) have collated the existing data on the temperature dependence of these electro-kinetic phenomena and found data which showed apparently conflicting behaviour as temperature increases (Reppert and Morgan 2003a; 2003b; Ishido and Mizutani 1981; Alekhin et al. 1984; Dunstan 1994). Vinogradov and Jackson (2015) attributed the observed contrasting behaviour to the pH, which was controlled in some studies and free to vary with temperature in others. This explanation not only explains the apparently conflicting behaviour, but is also supported by their data and conclusions.

Vinogradov and Jackson (2015) made electro-kinetic measurements on four sandstones for two salinities (0.01 mol/dm^3 and 0.5 mol/dm^3) as a function of temperature up to about 150°C. They found that the ζ was negative, decreasing in magnitude with increasing temperature at low ionic strength (0.01 mol/dm^3), and remaining independent of temperature at high ionic strength (0.5 mol/dm^3). They measured electrolyte pH and observed its decrease with increasing temperature at low salinity with no verifiable change with temperature at high salinity, which led to their assertion that the temperature dependence of the ζ can be explained by the temperature dependence of the pH. Vinogradov and Jackson (2015) carried out some basic modelling of only the ζ, finding it consistent with the approximate formulation by Revil et al. (1999a), which was implemented by Saunders et al. (2012) and discussed in Glover (2018).

The first theoretical model that was capable of providing both the ζ and C_{sp} efficiently for rock samples with individual pore microstructural parameters was reported by Glover et al. (2012a, b) who combined the Revil and Glover (1997, 1998) and Revil et al. (1999a) method for calculating the ζ from the electro-chemical relationships arising from the electrical double layer (EDL) with the modifications to the Helmholtz-Smoluchowski formula (*e.g.*, Glover (2015)) to take account of the pore microstructure (Glover and Déry 2010).

This paper modifies the Glover et al. (2012a, b) model so that it can be used to model the variation of C_{sp} and ζ as a function of temperature, recognizing that many of its input parameters are dependent on both temperature and salinity, and then attempts to model the Vinogradov and Jackson (2015) data.

2 The Model

The model I use in this study is a modified and re-implemented version of that of Glover et al. (2012a, b) incorporating all known temperature dependencies and implemented for the temperature range 0–150°C and for salinities between 10^{-5} and 1 mol/dm^3. Details of the model can be found in the text below, and the supplementary information (Glover 2026) includes the model implemented in Excel with active graphics.

2.1 Streaming Potential and Zeta Potential

The streaming potential of capillary tubes is known to be governed by the Helmholtz-Smoluchowski (HS) equation (e.g. Overbeek 1952; Hunter 1981; Maineult et al. 2004; Saunders et al. 2008), which is given in its simplest form by

$$C_s = \frac{\Delta V}{\Delta P} = \frac{\varepsilon_r \varepsilon_0 \zeta}{\eta_f \sigma_f^*} \quad (1)$$

where the streaming potential C_s (in V/m) is the ratio of the measured streaming potential ΔV (in V) to the applied fluid pressure difference ΔP (in Pa) that drives the fluid through the capillary tube. This value depends upon the electric permittivity of the pore fluid $\varepsilon_f = \varepsilon_r \varepsilon_0$ (in F/m), ε_r is the relative permittivity of the pore fluid (unitless), ε_0 is the electric permittivity of free space ($\approx 8.854 \times 10^{-12}$ F/m), the dynamic viscosity of the pore fluid η_f (in Pa.s), the pore fluid electrical conductivity σ_f^* (in S/m) and the zeta potential ζ (in V). The zeta potential is the electric potential on the shear plane when a part of the diffuse layer is transported by fluid flow. Equation 1 is valid for bundles of capillary tubes but is commonly applied to porous media including rocks even though it has never been validated for these media since there exists no independent measurement of the zeta potential for complex porous media.

The approach used in this work is a combination of fundamental theory and the use of empirical relationships. Theoretical models have been used for the heart of the model, i.e. to calculate the Debye screening length, Stern plane potential, zeta potential, surface conductance and streaming potential coefficient of the rock. Empirical relationships have been used to allow certain of the model's input parameters to vary as a function of temperature and fluid salinity instead of using input data from tables; these are the density, electrical conductivity, dynamic viscosity, the disassociation constant of water and the relative electric permittivity of the bulk fluid.

In parallel with the approach of other researchers, I have initially treated dielectric saturation (Pride and Morgan 1991) and visco-electric effects (Lyklema and Overbeek 1961; Hunter 1966; Pride and Morgan 1991) as negligible, the justification for which is given in Glover et al. (2012a, b).

The fluid conductivity in Eq. 1 has contributions from the bulk fluid and surface conduction. The latter depends both on the surface conductance and the microstructural properties of the rock (porosity, cementation exponent, grain size, etc.) as discussed in detail in Glover and Déry (2010). Consequently, Eq. 1 can be rewritten as (Morgan et al. 1989)

$$C_s = \frac{\Delta V}{\Delta P} = \frac{\varepsilon_r \varepsilon_0 \zeta}{\eta_f \left(\sigma_f + \frac{2\Sigma_s}{\Lambda} \right)} \quad (2)$$

where Σ_s is the specific surface conductance (in S) and Λ is a length scale characteristic of the pore microstructure (in m) introduced by Johnson et al. (1987). In this paper, I follow the approach of Glover and Déry (2010) by substituting the relationship of Revil and Cathless (1999) for the characteristic length scale ($\Lambda = d/(3(F-1))$) into Eq. 2 to obtain an equation for the streaming potential coefficient in terms of the mean grain diameter and formation factor of the rock giving Eq. 4 of Glover and Déry (2010)

$$C_s = \frac{\Delta V}{\Delta P} = \frac{d \varepsilon_f \zeta}{\eta_f \left(d \sigma_f + 6 \Sigma_s (F-1) \right)} \quad (3)$$

where d is the mean grain diameter (in m) and $F = \phi^{-m}$ is the formation factor of the rock. It is worthwhile noting that I have chosen to work with grain diameter in this modelling. However, other equations in Glover and Déry (2010) allow the modelling to be carried out as a function of pore radius or pore throat radius if one wishes, and these are also included in Fig. 1, which shows the main functional dependencies of the whole model.

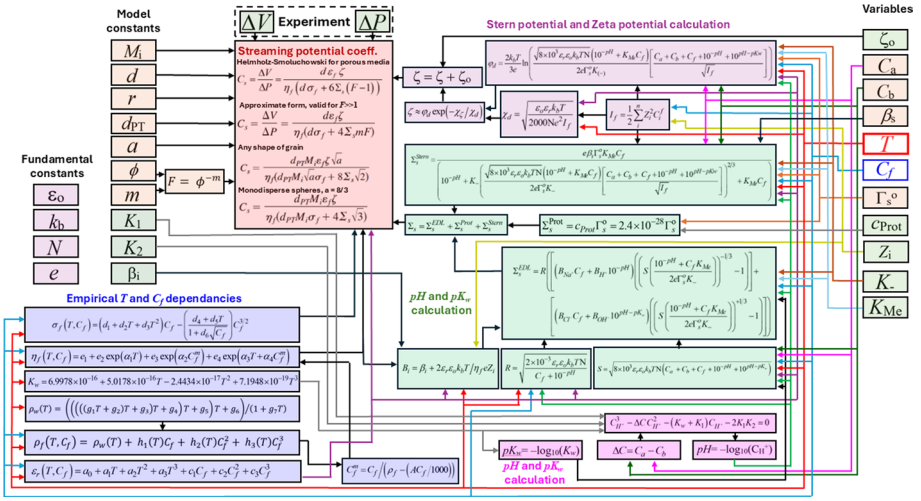

Fig. 1 Illustration of the main known influences in the model, which are described in Sect. 2 of this work, C_s (in V/m) is the ratio of the measured streaming potential ΔV (in V) to the applied fluid pressure difference ΔP (in Pa), $\varepsilon_f = \varepsilon_r \varepsilon_0$ (in F/m) is the electric permittivity of the pore fluid, ε_r is the relative permittivity of the pore fluid (unitless), ε_0 is the electric permittivity of free space ($\approx 8.854 \times 10^{-12}$ F/m), η_f (in Pa.s) is the the dynamic viscosity of the pore fluid, σ_f^* (in S/m) is the pore fluid electrical conductivity, and ζ (in V) is the zeta potential. The symbol Λ is a length scale characteristic of the pore microstructure (in m), d is the mean grain diameter (in m), r is the grain radius (in m), d_{PT} is the pore throat diameter (in m), m is the cementation exponent (no units), ϕ is the porosity or fluid fraction, a is a grain packing parameter whose value is 8/3 for spheres, M_i is the pore size to pore throat ratio for the ith packing, and $F = \phi^{-m}$ is the formation factor of the rock; α_i, a_i, c_i, e_i, h_i and d_i are various empirical parameters with different units, T is the operant temperature (in ^{o}C or K, depending in the equation (see text)), and C_f is the salinity of the bulk pore fluid (mol/dm^3) and C_f^m is the molality of that solution. K_w is the disassociation constant or water, and K_1 and K_2 are reaction coefficients of the reaction of CO_2 with water. C_a and C_b are the acid and base concentrations (in mol/dm^3) needed to be added to attain a given pH. $k_b = 1.38 \times 10^{-23}$ is Boltzmann's constant (J/K), $e = 1.602 \times 10^{-19}$ is the elementary charge (C), $N = 6.022 \times 10^{23}$ is Avogadro's constant (/mol), I_f is the ionic strength (mol/dm^3), Z_i is the valence of the i^{th} species, K_{Me}, is the binding constant for cation (usually sodium) adsorption on quartz, (-), $K_{(-)}$ or K_- is the disassociation constant for dehydrogenisation of silanol surface sites, Γ_s^0 is the surface site density (/m^2). φ_d is the Stern plane potential (V), χ_d is the Debye screening length (m), and $\chi_\zeta = 2.4 \times 10^{-10}$ is the shear plane distance, (m). The values of B_i are the equivalent ionic mobilities, and β_i are the ionic mobilities for each ion (both in m^2/s V), while β_s is the stern plane mobility. Σ_s is the surface conductivity, which is the sum of contributions from the EDL (Σ_s^{EDL}), from proton and electron conduction (Σ_s^{Prot}), and from the Stern layer (Σ_s^{Stern}), and where c_{Prot} is the proton surface conductance contribution rate.

The zeta potential and surface conductance have been calculated according to the model of Revil and Glover (1997, 1998) and Revil et al. (1999a). While the modelling has been carried out as a function of bulk fluid pH, it should be noted that the pH of the solution decreases in the diffuse layer as one approaches the mineral surface. Since the position of the shear plane is very close to the surface (a distance of about 2.4×10^{-10} m according to Revil and Glover (1997)), it is possible that the zeta potential would be significantly altered by the perturbation of the pH close to the mineral surface. So, there is the question over whether the bulk fluid property is the most appropriate one to use, or whether an adjusted pH value should be used in the calculation of the zeta potential.

However, I have no mechanism for making this adjustment because the surface conduction theory of Revil and Glover (1997) and Revil et al. (1999a) only accounts for pH variation in the bulk fluid. I am forced, therefore, to make the unsupported assumption that the

second-order pH effects close to the surface, including their effect on the zeta potential, are negligible for most pore fluid salinities.

The following subsections consider the development of the theoretical model, referencing those parts that have been drawn from previous work, followed by a subsection considering the main model parameters.

2.2 Theoretical Development

This subsection contains a full theoretical treatment of the temperature-dependent electrokinetic modelling of porous media presented in this work. Further supporting information can be found in Glover et al. (2012a, b). It is possible to calculate the streaming potential coefficient of reservoir rocks thanks to theoretical developments that began in 1997 (Revil and Glover 1997, 1998; Revil et al 1999a) and have been supplemented and modified (Glover and Déry 2010; Walker and Glover 2010). Here I combine them to provide a model for calculating the streaming potential coefficient as a function of 18 fundamental parameters including temperature, pore fluid concentration and pH, as well as rock parameters such as porosity, grain size, pore size and formation factor.

Examination of Eq. 2 shows that in order to calculate the streaming potential coefficient I need to obtain (i) the zeta potential, (ii) the electrical permittivity of the pore fluid, (iii) the viscosity of the pore fluid, (iv) the bulk fluid conductivity, (v) the surface conductance, and (vi) some measure of the characteristic length scale of the pores as discussed in Walker and Glover (2010). Here I use the grain size and Eq. 4 in Glover and Déry (2010), but one might equally well use the pore radius or the pore throat radius together with the respective equation in Glover and Déry (2010) instead.

The calculation method follows the following steps:

1. Calculation of the electrical conductivity of the pore fluid as a function of temperature and pore fluid concentration using the empirical model of Sen and Goode (1992a, 1992b).
2. Calculation of the relative permittivity of the pore fluid as a function of temperature and pore fluid concentration using the empirical model of Olhoeft (unpublished note, 1980, as mentioned by Revil et al., (1999b)).
3. Calculation of the mass density of the pore fluid as a function of salinity and temperature using the approach of Kell (1975) and Novotny and Söhnel (1988).
4. Calculation of the molality of the pore fluid as a function of salinity and temperature, with consequent calculation of the pore fluid viscosity as a function of temperature and pore fluid molality using the empirical model of Phillips et al. (1978).
5. Definition of the physical chemistry of the double layer based on the substrate (here silica) and the fluid (here aqueous solutions of NaCl in equilibrium with dissolved CO_2).
6. Calculation or imposition of the pH of the solution.
7. Calculation of the Debye screening length and the shear plane distance (Revil and Glover 1997, 1998; Revil et al. 1999a).
8. Calculation of the Stern plane potential (Revil and Glover 1997, 1998; Revil et al. 1999a).
9. Calculation of the zeta potential (Revil and Glover 1997, 1998; Revil et al. 1999a).
10. Calculation of the surface conductance (Revil and Glover 1997, 1998; Revil et al. 1999a).

11. Use of one of the forms of the modified Helmholtz-Smoluchowski equation given in Glover and Déry (2010), to finally calculate the streaming potential coefficient as a function of either (i) grain size, (ii) pore size, or (iii) pore throat size.

These steps are also given in the large summary diagram shown as Fig. 1. It will be noted that the use of the Helmholtz-Smoluchowski equation or modified Helmholtz-Smoluchowski equation (Eq. 1–3) is the last step in the streaming potential coefficient calculation, and has a temperature dependence solely because most of its input parameters have a temperature dependence.

It should be noted that this work considers how temperature change affects the physical properties of the fluid (viscosity, bulk conductivity, dielectric permittivity, pH etc.). However, in many field applications, temperature can also enhance chemical reactions, which can also modify fluid pH, ionic strength, conductivity, and therefore surface properties (Bernabé et al. 2003). These second-order effects can be very significant, but are specific to the particular applications and would need to be considered when modelling any specific field application.

There are a large number of input parameters in the model. Not all of them have a large impact upon the final streaming potential coefficient values, and this will be described in more detail in a further scientific contribution.

The input parameters fall into 5 groups:

(i) Fundamental constants (e.g. Boltzmann's constant and Avogadro's number).
(ii) Environmental conditions (e.g. temperature).
(iii) Fluid parameters (e.g. solute concentration, pH, pK_w, pK_1 *and* pK_2).
(iv) Rock microstructure parameters (e.g. formation factor, cementation exponent, porosity, grain size, etc.).
(v) Rock-fluid interface parameters, i.e. the electro-chemical parameters associated with surface adsorption reactions (e.g. pK_{me}, pK_{-}).

All the following modelling has been carried out as a function of pore fluid concentration assuming that the pore fluid is aqueous NaCl and that all changes in pH can be accommodated by the addition of small amounts of HCl or NaOH. Computations were carried out in Microsoft Excel from 10^{-5} to 10 mol/dm^3, with 5 points per decade, and in the range $4.5 \leq \text{pH} \leq 9$, where I note that for a silica surface the point of zero charge is about pH 3 ($\text{pH}_{pzc} \approx 3$), which the pH at which the EDL collapses. The methods for calculating the Stern plane potential and hence zeta potential used in this modelling become only approximately valid at $\text{pH} \leq 5$ (Revil et al. 1999a). Modelling has also been carried out as a function of temperature in the range $0\ ^\circ\text{C} \leq T \leq 100\ ^\circ\text{C}$. Extension beyond this range is only a matter of finding empirical relationships for the density, electrical conductivity, dynamic viscosity, dielectric permittivity and disassociation constant of the bulk fluid which are valid at the higher temperatures and also include pressure. There have been few studies on the effect of temperature upon those parameters entering the HS equation, the most important being those of Reppert and Morgan (2003a, 2003b).

Following the Roman numeral numbered list above, I consider each step in the following sub-sections, with the temperature dependence of some of the main input parameters shown in Fig. 2.

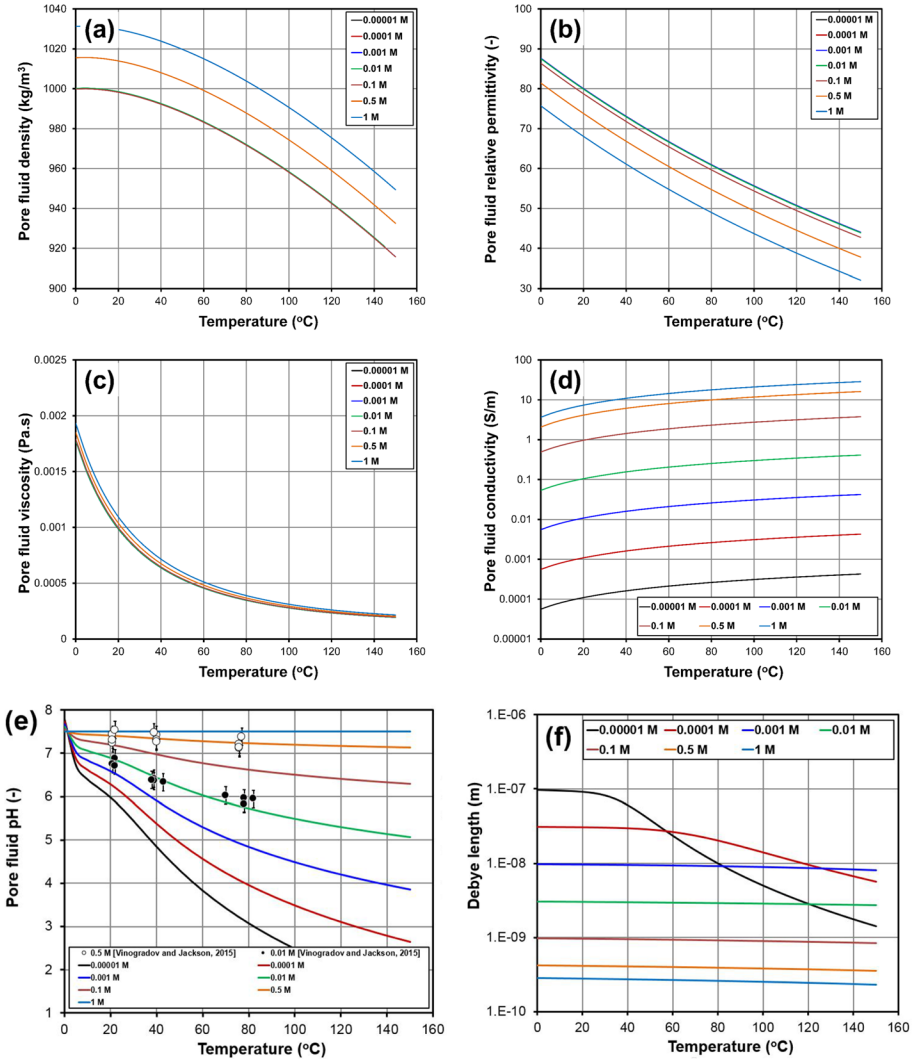

Fig. 2 The temperature and salinity dependencies of the main empirical parameters entering into the model: **a** pore fluid density, **b** pore fluid relative permittivity, **c** pore fluid viscosity, and **d** the pore fluid electrical conductivity, noting that the molality calculated in the model is only used to calculate the viscosity and is consequently not shown. In addition, I show two intermediate parameters calculated by the model and used to calculate the ζ and C_{sp}: **e** the pH as a function of temperature and salinity together with the measured values and uncertainties for $C_f = 0.01$ mol/dm^3 and $C_f = 0.5$ mol/dm^3, and (f) the Debye length

2.2.1 Pore Fluid Conductivity

I have used the corrected Sen and Goode (1992a, 1992b) empirical equation to provide the electrical conductivity of the bulk solution (in S/m) (noting the later reference provides an important correction to the equation)

$$\sigma_f(T, C_f) = \left(d_1 + d_2 T + d_3 T^2\right) C_f - \left(\frac{d_4 + d_5 T}{1 + d_6\sqrt{C_f}}\right) C_f^{3/2} \quad (4)$$

where $d_1 = 5.6$ (S. dm^3/m.mol), $d_2 = 0.27$ (S. dm^3/m.mol)/°C, $d_3 = -1.51 \times 10^{-4}$ (S. dm^3/m.mol)/°C^2, $d_4 = 2.36$ (S/m/(mol/dm^3)$^{3/2}$, $d_5 = 0.099$ (S/m/(mol/dm^3)$^{3/2}$/°C), $d_6 = 0.214$ ((mol/dm^3)$^{-1/2}$), T is in °C and C_f is the salinity of the bulk pore fluid (mol/dm^3). The variation of pore fluid conductivity with temperature is shown in Fig. 2d.

2.2.2 Pore Fluid Relative Electric Permittivity

Most researchers take a value of $\varepsilon_f = \varepsilon_r \varepsilon_0 = 80 \times 8.854 \times 10^{-12}$ F/m (e.g. Revil et al. 1999a, 1999b), which would correspond approximately to the bulk fluid being an aqueous solution at 25°C. However, I wish to model the streaming potential coefficient as a function of pore fluid salinity and temperature, both of which affect the value of the relative dielectric permittivity.

Consequently, I have determined the relative permittivity ε_r (no units) using Olhoeft's empirical equation (Olhoeft, unpublished note, 1980 mentioned in Revil et al. 1999b) as

$$\varepsilon_r(T, C_f) = a_0 + a_1 T + a_2 T^2 + a_3 T^3 + c_1 C_f + c_2 C_f^2 + c_3 C_f^3 \quad (5)$$

where $a_0 = 295.68$, $a_1 = -1.2283$ K^{-1}, $a_2 = 2.094 \times 10^{-3}$ K^{-2}, $a_3 = -1.41 \times 10^{-6}$ K^{-3}, $c_1 = -13.00$ dm^3/mol, $c_2 = 1.065$ (dm^3/mol)^2, $c_3 = -0.03006$ (dm^3/mol)^3, T is in kelvin and the equation is valid in the range from 273 to 373 K and C_f is the salinity of the bulk pore fluid in mol/dm^3. The permittivity *in vacuo* $\varepsilon_0 = 8.854 \times 10^{-12}$ F/m (Lide 2009).

The variation of pore fluid relative electric permittivity with temperature is shown in Fig. 2b.

It is debatable whether the value of ε_r for the bulk fluid is the most appropriate in this modelling. This is because the value of ε_r diminishes within the diffuse layer as one approaches the mineral surface (within a few angstroms), taking values as low as 5 near the Stern Plane (Grahame 1950). It would, perhaps, be more correct to use a smaller value of ε_r that would consider the reduction of the permittivity in the diffuse layer, which would give larger values of calculated zeta potential at high salinities, and which seem to be supported by experimental determinations (Jaafar 2009; Jaafar et al. 2009). Jaafar et al. found that above 0.4 mol/dm^3 (i.e. for Debye lengths less than 4.65×10^{-10} m) the zeta potential becomes constant and may even increase slightly, however they attributed the behaviour to surface charge density saturation not to dielectric saturation.

Unfortunately, at present there exists no theoretical model capable of providing us with a more appropriate effective permittivity value as such a value would depend on the microstructure of the rock. I have carried out some rudimentary CRIM based mixing calculations using the method of Iglesias and Peon Fernandez (2001) with a simplified rock microstructure and the results support the supposition that the dielectric saturation effect is negligible if the entire pore space contributes to the permittivity used by the modified H–S equation. Additionally, both Booth (1951) and Hunter (1966) provide a model of relative permittivity as a function of local field strength that indicates that the dielectric saturation effect is negligible for most bulk electrolyte solutions (Pride and Morgan 1991), but again, it is assumed that the whole of the pore fluid contributes to the permittivity to be used in the H–S equation.

One might consider that the appropriate permittivity to be used in the H–S equation is that at the shear plane. In which case it would be some exponential mixture of that at the Stern plane, which presumably approaches 5 after Grahame (1950), and that at the Bjerrum length from the surface, where the fluid ions are more affected by thermal agitation than the presence of the Stern layer, and where the permittivity approaches that given by Eq. 5 above. Under this hypothesis, permittivities of the order of 20 or less would be perfectly possible.

Finally, I note that if I replace the relative electric permittivity calculated by Eq. 5 in the model by the value of 5 for all salinities, the result is that the streaming potential coefficient is increased (becomes less negative) by an order of magnitude and zeta potential is decreased (becoming more negative) by approximately 15 mV, which is of the same order of magnitude as the experimental observations of zeta potential at high salinities made by Jaafar et al. (2009).

In this work, I have chosen to use the values of fluid permittivity for the bulk fluid (i.e. Eq. 5) because I considered the solution of the permittivity problem too large to include in this paper. However, I note that often the results of the model give positive zeta potentials at high salinities and low pHs that are not reproduced in experimental results. In these cases, I have added a constant zeta potential contribution, ζ_0, to that calculated by the model for all salinities. This ad hoc parameter improves the behaviour of the model at high salinity data, and is fully described in the Sect. 3. I expect that this parameter will not be required once the model contains a method for including the appropriate electric permittivity.

2.2.3 Pore Fluid Density

Pore fluid density is also required by the model, primarily to help calculate the pore fluid viscosity. The calculation is a two-step process. First, I calculate the density of pure water using the Kell equation (Kell 1975), which is given by

$$\rho_{\mathrm{w}}(T) = \frac{\left(\left(\left(\left(g_1 T + g_2\right)T + g_3\right)T + g_4\right)T + g_5\right)T + g_6\right)}{1 + g_7 T} \tag{6}$$

where ρ_{w} is the density of water in kg/m^3, T is the temperature (°C), and the empirical parameters are $g_1 = -2.8054253 \times 10^{-10}$ (in kg/m^3/°C^5), $g_2 = 1.0556302 \times 10^{-7}$ (in kg/m^3/°C^4), $g_3 = -4.6170461 \times 10^{-5}$ (in kg/m^3/°C^3), $g_4 = -0.0079870401$ (in kg/m^3/°C^2), $g_5 = 16.945176$ (in kg/m^3/°C), $g_6 = 999.83952$ (in kg/m^3), and $g_7 = 0.01687985$ (in/°C).

The density of the pore fluid containing a given amount of NaCl can be calculated using the Novotný and Söhnel (1988) equation

$$\rho_{\mathrm{f}}\left(T, C_{\mathrm{f}}\right) = \rho_{\mathrm{w}}(T) + h_1(T)C_{\mathrm{f}} + h_2(T)C_{\mathrm{f}}^2 + h_3(T)C_{\mathrm{f}}^3 \tag{7}$$

where; $\rho_{\mathrm{f}}\left(T, C_{\mathrm{f}}\right)$ is the solution density (g/dm^3), $\rho_{\mathrm{w}}(T)$ is the density of pure water (g/dm^3) at a given temperature T, C_{f} is the salinity of the solution in mol/dm^3, and the empirical parameters h_1 to h_3 are temperature-dependent functions, which can be found in Novotný and Söhnel (1988).

The variation of pore fluid density with temperature is shown in Fig. 2a.

2.2.4 Pore Fluid Viscosity

The dynamic viscosity η_f of the pore fluid (in Pa.s) was calculated using the Phillips et al. (1978) empirical equation

$$\eta_f(T, C_f) = e_1 + e_2 \exp(\alpha_1 T) + e_3 \exp(\alpha_2 C_f^m) + e_4 \exp(\alpha_3 T + \alpha_4 C_f^m) \quad (8)$$

where $e_1 = 4.95166 \times 10^{-5}$ Pa.s, $e_2 = 6.034658 \times 10^{-4}$ Pa.s, $e_3 = 9.703832 \times 10^{-5}$ Pa.s, $e_4 = 1.025107 \times 10^{-3}$ Pa.s, $\alpha_1 = -0.06653081$/°C, $\alpha_2 = 0.1447269$/molal, $\alpha_3 = -0.02062455$/°C, $\alpha_4 = 0.1301095$/molal, T is in °C and C_f^m is the molality of the bulk pore fluid. For weak solutions it is possible to say that $C_f^m \approx C_f$, and consequently to use salinity in mol/dm^3 in place of molality in Eq. 8. For stronger solutions it is necessary to calculate the density of the pore fluid and convert C_f into C_f^m using $C_f^m = C_f / (\rho_f - (AC_f/1000))$, where ρ_f is the pore fluid density in g/cm^3 and A is the atomic mass of the salt in g/mol (here for NaCl, $A = 58.44$ g/mol). Although the difference is small even at high salinities, I have implemented the conversion in our model for all salinities. The variation of pore fluid viscosity with temperature is shown in Fig. 2c.

As discussed in Glover et al. (2012a, b), visco-electric effects have been assumed to be negligible in accordance with the results of Lyklema and Overbeek (1961), Hunter (1966) and the interpretation of Pride and Morgan (1991). The separation at which the electrostatic interaction between two elementary charges is comparable in magnitude to the thermal energy scale is termed the Bjerrum length λ_b, and is given by $\lambda_b = e^2 / 4\pi\varepsilon_r\varepsilon_0 k_b T$. For an aqueous solution of NaCl and salinities less than about 0.4 mol/dm^3, the Bjerrum length remains constant at $\lambda_b = 7.16 \times 10^{-10}$ m, increasing to a value of 13.5×10^{-10} m at 3.98 mol/dm^3. The value of λ_b represents a threshold between a regime where fluid ions are more affected by thermal agitation than the presence of the Stern layer and the regime where the Stern layer dominates, and where the local field strength is sufficient to alter the viscosity of the fluid considerably. Figure 3 in Glover et al. (2012a, b) shows (i) the Bjerrum length λ_b, (ii) the Debye screening length χ_d, (iii) the thickness of the EDL (conventionally, twice the Debye screening length $2\chi_D$), and (iv) the shear plane distance $\chi_\zeta = 2.4 \times 10^{-10}$ m which has been taken from Revil and Glover (1997), all as a function of salinity. They showed that the Bjerrum length is greater than the EDL thickness for all salinities greater than about 0.5 mol/dm^3. This is the same as saying that inter-ionic electrostatic interactions are significant for the entire EDL, including all of its mobile fraction ($\chi > \chi_\zeta = 2.4 \times 10^{-10}$ m) for salinities greater than 0.5 mol/dm^3, and it is these electrostatic interactions that increase the fluid viscosity in the double layer. This viscosity perturbance is not taken account of in the Helmholtz-Smoluchowski equation which instead uses the bulk fluid viscosity rather than the local viscosity in the EDL. The bulk viscosity is perturbed negligibly by the local viscosity changes in such a thin layer near the mineral surface, which justifies our approach and that of previous authors (*e.g.* Pride and Morgan 1991).

2.2.5 Physical Chemistry of the EDL

The value of the Stern plane potential, and hence the zeta potential depends upon the surface chemistry which is different for different substrates. This paper confines itself to a silica surface. The reactions at a quartz surface in the presence of aqueous fluids has already been described well by many authors (*e.g.*, Iler 1979; Revil and Glover 1997, 1998; Revil et al. 1999a). There are two types of neutral surface group. The first is doubly coordinated siloxal $> Si_2O^0$, which can be considered inert, and other is singly coordinated

silanol $>SiOH^0$, which is reactive and gives $>SiOH_2^+$ when $pH < pH_{pzc}$, and $>SiO^-$ when $pH > pH_{pzc}$ (the symbol $>$ in the chemical formulae represents the silica crystal framework). The symbol pH_{pzc} represents the point of zero charge for the mineral, and is the pH at which $[>SiOH_2^+] = [>SiO^-]$, where square brackets indicate concentration. For silica $pH_{pzc} \approx 3$ (Lorne et al. 1999).

Following the approach of Revil et al. (1999a) this paper considers a 1:1 electrolyte with single valency anions and cations in the pH range 6–8 where the surface reactions can be written

$$>SiOH^0 \overset{K_{(-)}}{\Leftrightarrow} >SiO^- + H^+ \tag{9}$$

and

$$>SiOH^0 + Me^+ \overset{K_{Me}}{\Leftrightarrow} >SiOMe^0 + H^+ \tag{10}$$

where the metal cation is Me^+, and for most of our modelling it represents Na^+, though it might equally well represent K^+ or some other single valence cation. Note that the positive surface site $>SiOH_2^+$ does not occur in Eq. 9, 10 because at $pH > 6$ I have assumed that $(>SiOH_2^+) = 0$. Hence, there results three sites types; two neutral ($>SiOH^0$ and $>SiOMe^0$) and one negative ($>SiO^-$).

The position of the equilibrium in Eq. 9 is controlled by the disassociation constant for dehydrogenization of silanol surface sites $K_{(-)}$. If $K_{(-)}$ is large, Eq. 9 has an equilibrium towards the left, giving very many fewer $>SiO^-$ sites than $>SiOH^0$ sites, and vice versa. The position of the equilibrium in Eq. 10 is controlled by the binding constant for cation (sodium) adsorption on quartz K_{Me}. If K_{Me} is small, Eq. 10 has an equilibrium towards the left, where there are very many fewer $>SiOMe^0$ sites than $>SiOH^0$ sites, and vice versa. Hence, $K_{(-)}$ and K_{Me}, which are unitless, describe the relative concentrations of the three surface sites. The final parameter of interest is the total surface site density Γ_s^0 (in m^{-2}), which is the sum of the surface site densities for each of the three types of surface site.

2.2.6 Fluid pH

The last fluid property that is required is the fluid pH. Knowledge of the fluid pH is needed to calculate the surface conductance and Stern plane potential.

For an aqueous electrolyte in contact with the atmosphere the pH is defined by (a) the disassociation constant of water K_w, which varies with temperature, (b) the reaction of water with carbon dioxide from the atmosphere in a 2-step process, and (c) the addition of acid, and/or (d) the addition of a base.

The value of K_w varies with temperature. I have obtained an equation by fitting a polynomial to K_w data which was sourced from Lide (2009) and which is valid in the range $0\ °C \le T \le 100\ °C$

$$K_w = 6.9978 \times 10^{-16} + 5.0178 \times 10^{-16} T - 2.4434 \times 10^{-17} T^2 + 7.1948 \times 10^{-19} T^3 \tag{11}$$

It is worthwhile noting that this variation implies that the pH of pure water is 7.47 at 0°C, about 7 at 25 °C and 6.14 at 100°C. The relationship is likely approximately valid in the range $100°C \le T \le 150°C$ which is the limit of the data space explored in this model,

but it should be noted that the fit in this range is more approximate because it is an extrapolation outside the original Lide (2009) fitting data.

The reaction of water with atmospheric carbon dioxide occurs in two steps

$$H_2O + CO_2 \overset{K_1}{\Leftrightarrow} HCO_3^- + H^+, \text{ and} \tag{12}$$

$$HCO_3^- \overset{K_2}{\Leftrightarrow} CO_3^{2-} + H^+ \tag{13}$$

I have used equilibrium constants $K_1 = 10^{-7.53}$ and $K_2 = 10^{-10.3}$ after Wu et al. (1991) and Revil et al. (1999a). These two constants may depend upon temperature. I have assumed them to be independent of temperature. Implementing temperature dependencies of K_1 and K_2 is one area where this model could be improved.

The result of Eq. 11 and Processes 12 and 13 is that pure water in equilibrium with atmospheric carbon dioxide tends to be acidic. However, this initial acidity is reduced substantially when the fluid is equilibrated with the silica of the rock matrix. The process fluid can, of course, take any value of pH depending on the addition of an acid or a base (or both).

In this paper, I assume that the pH is imposed on the system. This choice is associated with the constraint that the model can be used with the data in Vinogradov and Jackson (2015) later in this paper as a case study. Modelling is only possible if the pH is measured during the experimental process and published with the other data. So many potentially useful datasets cannot be modelled because the experimental pH is either not measured, not recorded or not published. Consequently, the model assumes that a more acidic pH is obtained by adding HCl to the fluid in a concentration equal to C_a (in mol.L^{-1}), and a more basic pH is obtained by adding NaOH to the fluid in a concentration equal to C_b (in mol/dm^3). Each addition of acid or base will perturb the concentration of Cl^- ions and Na^+ ions in the solution, respectively. Both acid and base can be added together and their effect on pH will balance out, however, an augmentation of the concentration of Cl^- ions and Na^+ ions in the solution will still occur. This effect is taken account of in the model by the terms 10^{-pH} for hydrogen ions, $10^{(pH-pKw)}$ for hydroxyl ions, C_a for chloride ions that are added as HCl, and C_b for sodium ions that are added as NaOH. Hence, the model accounts for the addition of acid and base to the pore fluid solution to ensure that the ionic fluid concentrations in the model reflect those in a real pore fluid at a given pH.

The pH of the silica-H_2O-CO_2 system is defined by the cubic equation (Revil et al. 1999a)

$$C_{H^+}^3 - \Delta C\, C_{H^+}^2 - \left(K_w + K_1\right) C_{H^+} - 2K_1K_2 = 0 \tag{14}$$

where $\Delta C = C_a - C_b$ and $pH = -\log_{10}(C_H{}^+)$.

Consequently, there are two ways that a link can be built between acid and base concentrations and pH into the model. The first is to define the pH and then calculate the respective concentrations of acid and base required, which will then give us the augmentation in Cl^- and Na^+ ions in the pore fluid. If this approach is taken, it must assumed that either C_a or C_b is zero to ensure that the solution of Eq. 14 is unique. The second approach is to solve Eq. 14 for given values of C_a and C_b, and use the pH thus calculated in the model. I have implemented both approaches. The first is more convenient for fitting the model to experimental data where the pH of the pore fluid is known and has been used for the results

presented in this paper, while the second is more convenient if the recipe for the pore fluid is defined, for example, in experiment planning.

Figure 2e shows an example of the modelled pH as a function of temperature showing the greater functional dependence of the lower salinity solutions, and the agreement of the model with experimental data from Vinogradov and Jackson (2015).

2.2.7 Debye screening length and shear plane distance

The Debye screening length is given by

$$\chi_{\mathrm{d}} = \sqrt{\frac{\varepsilon_o \varepsilon_{\mathrm{r}} k_{\mathrm{b}} T}{2000 \mathrm{N} e^2 I_{\mathrm{f}}}} \tag{15}$$

where.

$k_{\mathrm{b}} = 1.38 \times 10^{-23}$	Boltzmann's constant	(J/K)	Lide (2009)
$e = 1.602 \times 10^{-19}$	elementary charge	(C)	Lide (2009)
$\mathrm{N} = 6.022 \times 10^{23}$	Avogadro's constant	(/mol)	Lide (2009)
$\varepsilon_0 = 8.854 \times 10^{-12}$	electrical permittivity *in vacuo*	(F/m)	Lide (2009)
ε_{r}	relative electrical permittivity	(–)	From Eq. 5
I_{f}	ionic strength	(mol/dm^3)	From Eq. 16
T	temperature	(K)	Model variable

The factor of 2000 arises due to the units for ionic strength being here mol/dm^3. This equation is often found cited with a 2 in place of the 2000, in which case the units for I_{f} would be mol/m^3.

The ionic strength is given by

$$I_{\mathrm{f}} = \frac{1}{2} \sum_{\mathrm{i}}^{n} Z_{\mathrm{i}}^2 C_{\mathrm{i}}^{\mathrm{f}} \tag{16}$$

In this work the acid and alkali contributions are usually small compared with that of the dissolved NaCl. Hence for the most common scenarios where $C_{\mathrm{f}} > 10^{-5}$ mol/dm^3 and $5 < \mathrm{pH} < 9$, it may be said that $I_{\mathrm{f}} \approx C_{\mathrm{f}}$.

There currently does not exist a method for independently evaluating the shear plane distance. Instead, a commonly followed approach is to use the value obtained by Revil and Glover (1997) when they fitted their model to the data of Scales et al. (1990), which is $\chi_\zeta = 2.4 \times 10^{-10}$ m.

The value of the Debye screening length generated in this work varied from 1.75×10^{-11} m to 9.68×10^{-8} m for $C_{\mathrm{f}} = 3.98$ mol/dm^3 and $T = 100$°C, and $C_{\mathrm{f}} = 10^{-5}$ mol/dm^3 and $T = 0$°C, respectively, both at pH = 7. The thickness of the diffuse layer may be considered to be approximately twice the Debye length. For $C_{\mathrm{f}} = 0.4$ mol/dm^3 at pH = 7 and $T = 25$°C Eq. 13 gives $2\chi_{\mathrm{d}} = 9.31 \times 10^{-10}$ m. Since $2\chi_{\mathrm{d}} \geq \chi_\zeta$, a significant amount of the double layer (74.2%) is moved during electro-kinetic coupling, and this amount increases swiftly to approach 100% of the double layer for lower pore fluid concentrations. The condition that $2\chi_{\mathrm{d}} = \chi_\zeta$ is reached at a concentration of 3.395 mol/dm^3, but streaming potentials are possible at higher salinities because the EDL decays away exponentially, ensuring that the arbitrary limit on its size given by $2\chi_{\mathrm{d}}$ is not a true reflection on the extent of the EDL.

The EDL extends beyond $2\chi_d$, but very weakly, and it is this weak portion of the EDL that gives rise to the small streaming potential coefficients at concentrations greater that 3.395 mol/dm^3.

Figure 2f shows the variation of the Debye length with salinity and temperature, capturing the smaller Debye lengths for the higher salinity fluids, and noting that there is only a small decrease in Debye length with temperature up to 150°C for most fluids (those with $C_f > 5 \times 10^{-4}$ mol/dm^3). However, there is a much more pronounced decrease in Debye length with increase in temperature for very low salinity solutions ($C_f = 10^{-4}$ mol/dm^3 and $C_f = 10^{-5}$ mol/dm^3) which we associate later with the cause for the apparently positive streaming potential coefficients for these low salinities.

2.2.8 Stern Plane Potential

The Stern plane potential was calculated using the techniques described in Revil and Glover (1997) and in Revil et al. (1999a), and is given by

$$\varphi_d = \frac{2k_bT}{3e} \ln\left(\frac{\sqrt{8 \times 10^3 \varepsilon_r \varepsilon_0 k_b T N}\left(10^{-pH} + K_{Me} C_f\right)}{2e\Gamma_s^0 K_{(-)}} \left[\frac{C_a + C_b + C_f + 10^{-pH} + 10^{pH-pKw}}{\sqrt{I_f}} \right] \right) \tag{17}$$

where:

$k_b = 1.38 \times 10^{-23}$	Boltzmann's constant	(J/K)	Lide (2009)
$e = 1.602 \times 10^{-19}$	elementary charge	(C)	Lide (2009)
$N = 6.022 \times 10^{23}$	Avogadro's constant	(/mol)	Lide (2009)
$\varepsilon_0 = 8.854 \times 10^{-12}$	electrical permittivity *in vacuo*	(F/m)	Lide (2009)
$Z_i = 1$	valence of the ionic species *i*	(–)	Lide (2009)
ε_r	relative electrical permittivity	(–)	From Eq. 5
I_f	ionic strength	(mol/dm^3)	From Eq. 16
K_{Me}	binding constant for cation (usually sodium) adsorption on quartz	(–)	Model variable
$K_{(-)}$	disassociation constant for dehydrogenisation of silanol surface sites	(–)	Model variable
C_a	acid concentration	(mol/dm^3)	From Eq. 14
C_b	base concentration	(mol/dm^3)	From Eq. 14
Γ_s^0	surface site density	(/m^2)	Model variable
C_f	concentration of the solution	(mol/dm^3)	Model variable
pH	pH	(–)	Model variable
T	temperature	(K)	Model variable

This equation is the same as that developed in Glover et al. (2012a, b) but is used here to explore the temperature dependence of the Stern potential which is both explicit and hidden in the temperature dependence of many of its other parameters.

While the fundamental constants are known to great accuracy, there is some considerable uncertainty over the exact value of other parameters such as K_{Me}, $K_{(-)}$, and Γ_s^0 as discussed earlier, in Revil et al. (1999a), and in detail in Sect. 3 below.

It will be noted that Eq. (17), though the same as that in Glover et al. (2012a, b) is more comprehensive than the version given in Revil et al. (1999a). This is because the addition of the C_b and 10^{pH-pKw} terms allow it to be applied for a full range of pH values, whereas strictly the equation in Revil et al., (1999a) is only valid for pH < 7.

This work choses to obtain the temperature dependence of pH from the temperature dependence of K_w. This allows the temperature dependence of pH and p*K*w to be calculated for a given set of C_a and C_b, K_1 and K_2, which makes the calculation more generally applicable. Use of a direct empirical fit to the pH(T) relationship would be tied to a fixed set of ΔC, K_1 and K_2 values, which would reduce its utility as a model. Such a general approach is needed when many of the input parameters to the model (and to Eq. 17) are themselves temperature-dependent; not to do so risks not including latent functionalities.

The theoretical values of Stern plane potential arrived at in this work were between −181.6 mV and 15.1 mV for $C_f = 10^{-5}$ mol/dm^{3}and $T = 100$°C, and $C_f = 3.98$ mol/dm^{3}and $T = 0$ °C, respectively, and both with pH = 7, $pK_{Me} = 7.5$, $pK_{(-)} = 7$, and $\Gamma_s^0 = 10$ sites/nm^3.

2.2.9 Zeta Potential

The electrical potential φ in the EDL has, approximately, an exponential distribution given by $\varphi \approx \varphi_d \exp\left(-\chi / \chi_d\right)$, where φ_d is the Stern plane potential (V), χ_d is the Debye screening length (m) and χ is the distance from the mineral surface (m). It is, in fact, the solution of the linearised approximation of the Poisson-Boltzmann equation for the EDL (Eq. 35 of Revil and Glover (1997)). The exponential form of Eq. 18 is often called the Debye-Hückel approximation.

The zeta potential can then be calculated using (Revil and Glover 1997, 1998; Revil et al. 1999a)

$$\zeta \approx \varphi_d \exp\left(-\chi_\zeta / \chi_d\right) \tag{18}$$

where.

φ_d	Stern plane potential	(V)	From Eq. 17
χ_d	Debye screening length	(m)	From Eq. 15
$X_\zeta = 2.4 \times 10^{-10}$	shear plane distance	(m)	Revil and Glover (1997)

The theoretical values of the zeta potential arrived at in this work were between −201 mV and zero for $C_f = 10^{-5}$ mol/dm^3 and $T = 100$°C, and $C_f =$ mol/dm^3 and $T = 0$°C, respectively, and both with pH = 7, $pK_{Me} = 7.5$, $pK_{(-)} = 7$, and $\Gamma_s^0 = 10$ sites nm^{-3}.

2.2.10 Surface Conduction

The surface conductance was also calculated using the techniques described in Revil and Glover (1997; 1998) and in Revil et al. (1999a). The surface conductance is given by

$$\Sigma_s = \Sigma_s^{EDL} + \Sigma_s^{Prot} + \Sigma_s^{Stern} \tag{19}$$

where

$$\Sigma_s^{\text{Stern}} = \frac{e\beta_s\Gamma_s^0 K_{\text{Me}} C_f}{\left(10^{-\text{pH}} + K_- \left(\frac{\sqrt{8\times10^3\varepsilon_r\varepsilon_0 k_b TN}\left(10^{-\text{pH}} + K_{\text{Me}}C_f\right)}{2e\Gamma_s^0 K_-}\left[\frac{C_a + C_b + C_f + 10^{-\text{pH}} + 10^{\text{pH}-pK_w}}{\sqrt{I_f}}\right]\right)^{2/3} + K_{\text{Me}}C_f\right)} \tag{20}$$

and where

$$\Sigma_s^{\text{EDL}} = R\left(\left[\left(B_{\text{Na}^+}C_f + B_{\text{H}^+}10^{-\text{pH}}\right)\left(\left(S\left(\frac{10^{-\text{pH}} + C_f K_{\text{Me}}}{2e\Gamma_s^0 K_-}\right)\right)^{-1/3} - 1\right)\right] + \left[\left(B_{\text{Cl}^-}C_f + B_{\text{OH}^-}10^{\text{pH}-pK_w}\right)\left(\left(S\left(\frac{10^{-\text{pH}} + C_f K_{\text{Me}}}{2e\Gamma_s^0 K_-}\right)\right)^{+1/3} - 1\right)\right]\right) \tag{21}$$

where

$$R = \sqrt{\frac{2\times10^{-3}\varepsilon_r\varepsilon_0 k_b TN}{C_f + 10^{-\text{pH}}}} \tag{22}$$

and where;

$$S = \sqrt{8\times10^3\varepsilon_r\varepsilon_0 k_b TN\left(C_a + C_b + C_f + 10^{-\text{pH}} + 10^{\text{pH}-pK_w}\right)} \tag{23}$$

In Eq. 20 to Eq. 23 $\text{pH} = -\log_{10}\left(C_H^+\right)$, $pK_w = -\log_{10}\left(K_w\right)$, and K_w is the disassociation constant of water that is given by Eq. 9. In Eq. 21, The terms B_i are the equivalent ionic mobilities for each ion, where $B_i = \beta_i + 2\varepsilon_r\varepsilon_0 k_b T/\eta_f e Z_i$, and where β_i is the ionic mobility of each ion.

$\beta_{Na}{}^+ = 5.20\times10^{-8}$	Ionic mobility of sodium ions	(m^2/s V)	Crow (1988)
$\beta_H{}^+ = 3.63\times10^{-7}$	Ionic mobility of hydrogen ions	(m^2/s V)	Crow (1988)
$\beta_{Cl}{}^- = 7.90\times10^{-8}$	Ionic mobility of chloride ions	(m^2/s V)	Crow (1988)
$\beta_{OH}{}^- = 2.05\times10^{-7}$	Ionic mobility of hydroxyl ions	(m^2/s V)	Crow (1988)

The ionic mobility controls the size of the electro-migration contribution to the diffuse layer conductance, while the term $2\varepsilon_r\varepsilon_0 k_b T/\eta_f e Z_i$ controls the size of the electro-osmotic contribution to the diffuse layer conductance. The equivalent ionic mobilities B_i thus account for both processes.

Although the contribution from the diffuse layer $\Sigma_s{}^{\text{EDL}}$ was shown to be negligible by Revil and Glover (1998) for a small range of parameters, I have implemented it in full in this model to be as complete as possible.

The contribution of the protons (and electrons) is thought to involve conduction along the surface only (O'Konski 1960) and to be a function of surface site density but not of salinity (Revil and Glover 1998). Watillon and de Backer (1970) have found that the surface conduction for a silica glass capillary full of pure water is $\Sigma_s = 2.4\times10^{-9}$ S. Given that Revil and Glover (1998) have found that $\Gamma_s{}^0 = (1.0\pm0.06)\times10^{19}$ sites/m^2 for the same data,

I have assumed linearity and used the following formulation to calculate the proton contribution to the surface conductance

$$\Sigma_s^{\text{Prot}} = c_{\text{Prot}}\Gamma_s^0 = 2.4\times10^{-28}\Gamma_s^0 \tag{24}$$

where $c_{\text{Prot}}=2.4\times10^{-28}$ Sm^2/site is the proton surface conductance contribution rate. All the other parameters in Eq. 16 to Eq. 24 have already been described except β_s, which is the ionic surface mobility (in m^2/s V). I have used $\beta_s=5\times10^{-9}$ m^2/s V from Revil et al. (1998).

The theoretical values of the surface conductance arrived at in this work were between 8.76×10^{-9} S and 2.64×10^{-9} S for $C_f=3.98$ mol/dm^3 and $T=100$°C, and $C_f=10^{-5}$ mol/dm^3 and $T=0$°C, respectively, and both with pH=7, $pK_{\text{Me}}=7.5$, $pK_{(-)}=7$, and $\Gamma_s^0=10$ sites nm^{-3}.

2.2.11 Streaming Potential Coefficient

The streaming potential coefficient has been calculated from the values of the pore fluid dielectric permittivity $\varepsilon_f=\varepsilon_r\varepsilon_0$, zeta potential ζ, bulk fluid conductivity σ_f, pore fluid viscosity η_f, and surface conductance Σ_s, all calculated previously, together with the grain diameter d, cementation exponent m, and formation factor $F=\phi^{-m}$, where ϕ is the porosity, using Eq. 4 of Glover and Déry (2010)

$$C_s = \frac{\Delta V}{\Delta P} = \frac{d\,\varepsilon_f\,\zeta}{\eta_f\left(d\,\sigma_f + 6\,\Sigma_s\,(F-1)\right)} \tag{25}$$

The grain diameter d, cementation exponent m, formation factor F, and porosity ϕ describe the microstructure of the rock matrix, and allow the previous modelling to be applied to real geological materials, such as rocks, sands and soils.

2.2.12 Influences

In reading the complex and interwoven functional relationships described in the last eleven subsections, it will be realised that the model is a web of influences that contain feedback loops, and where any single parameter (salinity, for example) is the input to many of the operating equations. The value of both C_f and the prime variable in this modelling, Temperature T are both inputs to 10 different operating equations, each of which often interact with each other. This makes the model extremely difficult to predict. This complexity is illustrated by the main summary diagram shown as Fig. 1.

3 The Parameters

Since the model presented in this paper is a temperature-dependent modification of that given by Glover et al. (2012a, b), it shares a similar high number of independently adjustable parameters (22 $_{\text{cf}}$ Glover et al.'s (2012a, b) 18), but as before many are either model variables or are fixed by independent measurements.

3.1 Model Variables

Temperature T, salinity C_f, and pH are all considered to be model variables. These variables are either fixed, or the model is run as a function of one or more of them. For the modelling of the Vinogradov and Jackson (2015) both salinity and pH are known, and are treated as experiment (sample) fixed parameters.

3.2 Rock-Specific Parameters

Grain diameter d, porosity ϕ, grain radius r, pore throat diameter d_{PT}, grain packing parameter a, the pore size to pore throat ratio M_i, cementation exponent m, and formation factor F, are all rock-specific microstructural parameters which are fixed by whatever rock sample one wishes to model.

3.3 Fluid-Specific Parameters

The four effective ionic mobilities in a given aqueous fluid are independently available from electrochemical research (*e.g.*, Crow 1988). The equilibrium constants $K_1 = 10^{-7.53}$ and $K_2 = 10^{-10.3}$ are likewise known from studies made on the silica-H_2O-CO_2 system (*e.g.,* Wu et al. 1991).

The values of C_a and C_b that are added to attain a given pH are other fixed fluid-related parameters, while valence Z_i is also defined for the specific fluid being modelled.

3.4 Key Parameters

There is more uncertainty over the value of the six remaining variables; each is discussed at greater length below.

3.4.1 Surface Site Density

The range of this parameter for silica surfaces varies considerably because silica surfaces can exist in a variety of forms, from amorphous silica, for which values of 4.6 sites/nm^2 (Iler 1979), 5 sites/nm^2 (Park and Regalbuto 1995) and 6 sites/nm^2 (Kosmulski 1996) have been published, to crystalline silica for which both 9.6 sites/nm^2 and 6 sites/nm^2, for the (001) and (010) crystallographic planes, respectively, have been measured (Hiemstra and Van Riemsdijk 1990). For crushed quartz, a lower value of 2.6 sites/nm^2 was obtained by Jørgensen and Jensen (1967) which was attributed to the crushing process by Revil et al. (1999a), while at high pH values and during dissolution values as high as 25 sites/nm^2 are theoretically possible and confirmed by acid/base titration measurements at high pH values (Tadros and Lykelma 1969; Yates and Healy 1976).

Revil and Glover (1998) found a value of 10.0 ± 0.6 sites/nm^2 while modelling the data of Watillon and de Backer (1970) which was made using an aqueous KNO_3 electrolyte at pH = 6.8 in a silica glass capillary. Later, Revil et al. (1999a) refined the surface site density to 9.3 sites nm^{-2} modelling the same data, and also stated that they consider that the value should generally lie in the range 5 to 10 sites/nm^2 providing pH $\leq$ 8.

Glover et al. (2012a, b) carried out modelling varying this parameter between 2.5 and 25 sites/nm^2 for a NaCl pore fluid with a pH between 5 and 8 while keeping all other parameters constant (pK_{me} = 7.5, p$K_{(-)}$ = 7.1, $\chi_\zeta = 2.4 \times 10^{-10}$ m, $c_{Prot} = 2.4 \times 10^{-28}$ Sm^2/site $\beta_s = 5 \times 10^{-9}$ m^2/s V, $d = 2 \times 10^{-5}$ m, $m = 1.8$, $\phi = 0.2$) and found that it has the effect of changing the streaming potential negligibly for $C_f > 0.01$ mol/dm^3 NaCl, and diminishing it by up to one order of magnitude for $C_f < 0.01$ mol/dm^3 NaCl. They noted that the strength of the low salinity effect is dependent upon the microstructural properties of the rock (grain size, formation factor, porosity etc.). In addition, they noted that the change from 2.5 to 25 sites nm^{-2} reduced the sensitivity of the streaming potential coefficient to pH in the range 5 to 8.

In this work, a value of 10 sites/nm^2 has been used.

3.4.2 Binding Constant for Cation Adsorption

The value of this parameter is not well known, partly because it is rarely measured and varies according to which cation is dominant. Existing data for silica give pK_{me} (Li^+) = 7.8 and pK_{me} (Na^+) = 7.1 (Dove and Rimstidt 1994), pK_{me} (Li^+) = 7.7, pK_{me} (Na^+) = 7.5 and pK_{me} (Cs^+) = 7.2 (Kosmulski 1996), and pK_{me} (Na^+) = 3.25 and pK_{me} (K^+) = 2.8 (Revil et al. 1999a).

Glover et al. (2012a, b) carried out modelling varying this parameter between 3.25 and 7.5 for a NaCl pore fluid with a pH between 5 and 8 while keeping all other parameters constant ($\Gamma_s^0 = 10$ sites/nm^2, p$K_{(-)}$ = 7.1, $\chi_\zeta = 2.4 \times 10^{-10}$ m, $c_{Prot} = 2.4 \times 10^{-28}$ Sm^2/site, $\beta_s = 5 \times 10^{-9}$ m^2/s V, $d = 2 \times 10^{-5}$ m, $m = 1.8$, $\phi = 0.2$) and found that it has little effect $C_f < 0.01$ mol/dm^3 NaCl, but seems to have a drastic effect in the range $0.01 > C_f > 2$ mol/dm^3 NaCl where positive streaming potentials are predicted as p$K_{me} \rightarrow 3.25$. They concluded that it is clearly important to understand the sensitivity of this parameter.

In this work, a value of pK_{me} = 7.5 has been used.

3.4.3 Disassociation Constant for Dehydrogenization

Once again, the actual value of this parameter is not well known. Experimental values include p$K_{(-)}$ = 6.8 (Dove and Rimstidt 1994), p$K_{(-)}$ = 6.5 (Kosmulski 1996), and p$K_{(-)}$ = 7.5 (Hiemstra and van Riensdijk, 1990). A modelling study by Rustad (1998) predicted that p$K_{(-)}$ = 8.5. Revil et al. (1999a) have used p$K_{(-)}$ = 7.4 to 7.5 in their modelling, while Glover et al. (2012a, b) used p$K_{(-)}$ = 7.7.

Glover et al. (2012a, b) also carried out modelling varying p$K_{(-)}$ between 6.5 to 8.5 for a NaCl pore fluid with a *pH* between 5 and 8 while keeping other parameters constant ($\Gamma_s^0 = 10$ sites/nm^2, pK_{me} = 7.5, $\chi_\zeta = 2.4 \times 10^{-10}$ m, $c_{Prot} = 2.4 \times 10^{-28}$ Sm^2/site, $\beta_s = 5 \times 10^{-9}$ m^2/s V, $d = 2 \times 10^{-5}$ m, $m = 1.8$, $\phi = 0.2$) and found that increasing p$K_{(-)}$ decreases the streaming potential coefficient for all salinities except those greater than 1 mol/dm^3. The decrease was found to be small for solutions with pH 7 and pH 8 (about a twofold decrease), but is larger for pH 6 and leads to more than an order of magnitude for pH 5.

In this work, a value of p$K_{(-)}$ = 7.7 has been used.

3.4.4 The shear Plane Distance

There exist few independent measurements of the shear plane distance χ_ζ. Smith (1976) found $\chi_\zeta = 5.0 \times 10^{-10}$ m, while Revil and Glover (1997) used χ_ζ as an adjustable parameter in their model to obtain $\chi_\zeta = 2.4 \times 10^{-10}$ m. A similar fitting procedure was used by Ishido and Mizutani (1981) to obtain $\chi_\zeta = 2.0 \times 10^{-9}$ m.

It should be noted that Revil et al. (1999a) used $\chi_\zeta = 0$ m, which corresponds to the shear plane and Stern plane being co-located (*i.e.*, fluid flow transports the entire diffuse layer). While this is a useful tool to reduce the number of parameters in the model by one, Glover et al. (2012a, b) considered it to be unduly restrictive because the modelled streaming potential coefficient at high salinities is sensitive to changes in this parameter.

Glover et al. (2012a, b) also carried out modelling varying χ_ζ between 2.4×10^{-11} m and 2.4×10^{-9} m for a NaCl pore fluid with a pH between 5 and 8 while keeping the other parameters constant ($\Gamma_s^o = 10$ sites/nm^2, $pK_{me} = 7.5$, $pK_{(-)} = 7.1$, $c_{Prot} = 2.4 \times 10^{-28}$ Sm^2/site, $\beta_s = 5 \times 10^{-9}$ m^2/s V, $d = 2 \times 10^{-5}$ m, $m = 1.8$, $\phi = 0.2$) and found that increasing χ_ζ reduces the streaming potential coefficient curves for all four *pH*s, but only negligibly for χ_ζ changing from 2.4×10^{-11} m to 2.4×10^{-10} m, but reduces the streaming potential by half an order of magnitude for all four *pH*s when augmenting the value further to 2.4×10^{-9} m, which provided model curves that were an extremely good fit to the data.

The modelling in this paper sets $\chi_\zeta = 5 \times 10^{-9}$ m.

3.4.5 Contributions to Surface Conduction

The surface conduction has contributions from so-called proton conduction, from the Stern plane and from the diffuse layer. The contributions from the Stern plane and diffuse layers are not input parameters as they are calculated in the model. Although the contribution from the so-called proton conduction is also calculated in the model, it is directly controlled by the values of the proton surface conductance contribution rate c_{prot} and the density of surface sites (discussed in subSect. 3.4.1. above). Consequently, c_{prot} may be considered to be an important input parameter.

Watillon and de Backer (1970) carried out experimental determinations using pure water on silica glass at 20–25°C, obtaining $c_{Prot} = 2.4 \times 10^{-28}$ Sm^2/site, which gives a value of $\Sigma_s^{Prot} = 2.4 \times 10^{-9}$ S using Eq. 24 and $\Gamma_0 = 10$ sites/nm^2, coinciding with the value used by Revil et al. (1999a) and Glover et al. (2012a, b).

Glover et al. (2012a, b) carried out a brief sensitivity of this parameter, increasing it from 2.4×10^{-29} m to 2.4×10^{-27} m for a NaCl pore fluid with a *pH* between 6 and 8 while keeping other parameters constant ($\Gamma_s^o = 10$ sites/nm^2, $pK_{me} = 7.5$, $pK_{(-)} = 7.1$, $\chi_\zeta = 2.4 \times 10^{-10}$ m, $\beta_s = 5 \times 10^{-9}$ m^2/s V, $d = 2 \times 10^{-5}$ m, $m = 1.8$, $\phi = 0.2$). They found that increasing c_{prot} has negligible effect upon the streaming potential for fluids with $C_f > 0.01$ mol/dm^3 NaCl, pH 5–8. However, there is a significant reduction in the streaming potential for fluids where $C_f < 0.01$ mol/dm^3 NaCl, pH 5–8. Glover et al. (2012a, b) concluded that increasing c_{Prot} has a similar effect as changes to rock microstructural properties which enhance the role of surface conduction, with both increasing the effect of surface conduction on the streaming potential coefficient.

The modelling in this paper uses $c_{Prot} = 2.4 \times 10^{-28}$ Sm^2/site.

Table 1 General modelling parameters

Parameter	Units	Value	Source
Temperature	°C, K	Modelling variable	Imposed
Salinity, C_f	M	Modelling variable	Imposed
pH	(–)	Modelling variable	Calculated in the model
Pore fluid density, ρ_f	kg/m^3	Empirical	Lide (2009)
Pore fluid molality, b_f	mol/kg	Empirical	Lide (2009)
Pore fluid viscosity, η_f	Pa.s	Empirical	Phillips et al. (1978)
Pore fluid relative permittivity, ε_f	(–)	Empirical	Revil et al. (1999b)
Pore fluid electrical conductivity, σ_f	S/m	Empirical	Sen and Goode (1992a, 1992b)
Disassociation constant of water pK_w	(–)	Empirical	Lide (2009)
Surface site density Γ_0	sites/nm^2	10	Revil and Glover (1998)
Binding constant for cation (Na^+) adsorption on quartz pK_{Me}	(-)	7.5	Kosmulski (1996)
Disassociation constant for dehydrogenization of silanol $pK_{(-)}$	(–)	7.7	see range in Glover et al. (2012a, b)
Shear plane distance χ_ζ	m	5.0×10^{-9}	see range in Glover et al. (2012a, b)
Protonic surface conduction Σ_s^{prot}	S	2.4×10^{-9}	Revil et al. (1999b)
Ionic Stern plane mobility β_s	m^2/s V	5.0×10^{-9}	see range in Glover et al. (2012a, b)
Ionic mobility of Na^+ ions $\beta_{Na}{}^+$	m^2/s V	5.2×10^{-8}	Crow (1998)
Ionic mobility of H^+ ions $\beta_H{}^+$	m^2/s V	36.3×10^{-8}	Crow (1998)
Ionic mobility of Cl^- ions $\beta_{Cl}{}^-$	m^2/s V	7.9×10^{-8}	Crow (1998)
Ionic mobility of OH^- ions $\beta_{OH}{}^-$	m^2/s V	20.5×10^{-8}	Crow (1998)
Zeta potential offset ζ_0	mV	−9.5	Vinogradov and Jackson (2015)
Modal grain size d_{grain}	m	1.3×10^{-4}	St. Bees Sandstone 1Vinogradov and Jackson (2015)
Porosity ϕ	(–)	0.19	
Cementation exponent m	(–)	1.74	

3.4.6 The Surface Mobility

There is significant uncertainty over the value of the surface mobility (Glover et al. 2012a, b). Watillon and de Backer (1970) has used value of $\beta_s = 4\times10^{-9}$ m^2/s V in modelling their data, while Revil and Glover (1998) used a value of 5.14×10^{-9} m^2/s V that was derived by fitting their theory to shaly sand data. Later, both Revil et al. (1999a) and Glover et al. (2012a, b) used a value of 5×10^{-9} m^2/s·V in their modelling. These surface mobilities are approximately ten times less than the mobility of Na^+ in water ($\beta_f^{(+)} = 5.2\times10^{-8}$ m^2/sV) according to Crow (1988) and Waxman and Smits (1968).

It is known that the streaming potential coefficient is extremely insensitive to changes in the surface mobility in this restricted range. Unreasonably high surface mobilities, four orders of magnitude higher, are required any effect upon the modelled streaming potential coefficient can be noted (Glover et al. 2012a, b).

In this modelling, a value of surface mobility $\beta_s = 5\times10^{-9}$ m^2/s V has been used.

4 Implementation

The model begins by calculating important pore fluid parameters as a function of temperature using the well-understood empirical and theoretical relationships set out in the last section: (i) density ρ_f, (ii) molality b_f, (iii) relative permittivity ε_f, (iv) viscosity η_f, (v) electrical conductivity σ_f, (vi) Debye length χ_D, and (vii) pK_w. The values of pH and pOH can then be calculated. The value of pH is particularly important not only because the ultimate values of C_{sp} and ζ are extremely sensitive to this parameter, but the pH varies with both temperature and fluid salinity. The temperature dependence of most of these input parameters are shown in Fig. 2, while Table 1 shows the source of the relationships used to obtain them.

Each of these input parameters undergoes significant variation over the range of salinities (10^{-5} to 1 mol/dm^3) and temperatures (0 to 150°C) considered in this paper. Pore fluid density, molality, relative permittivity, viscosity and electrical conductivity undergo a change of −8.4%, −9.2%, −49.8%, 89.1%, and + 664%, respectively, over the temperature interval 0 to 150°C. In addition, the water product coefficient pKw (and hence pH) also varies with temperature, leading to a change of + 22% in pH over the same temperature range for a 0.01 mol/dm^3 NaCl solution, which becomes less for fluids with a larger salinity and greater for lower salinity fluids (Fig. 2e).

The modelled temperature dependence of electrolyte pH accounts for water dissociation, addition of acid/base, and CO_2 dissolution in water due to fluid equilibration with atmospheric CO_2. The Vinogradov and Jackson (2015) experimental data were obtained in a closed systems without any access to atmospheric CO_2, thus no change in pH associated with CO_2 dissolution was expected during the experiment but the fluids would have been equilibrated with the atmosphere before the experiment started. Vinogradov and Jackson (2015) noted experimentally that the pH of brines of high salinity (0.5 mol/dm^3) did not change with temperature in the range 20–80°C, while lower salinity brines reduced in pH, exemplified by that of 0.01 mol/dm^3 NaCl brine which decreased from about pH 6.5 to pH 5.5 in the range 20°C–80°C. It is interesting to note that our model provides the same behaviour as found experimentally by Vinogradov and Jackson (2015).

The Stern potential can be calculated using the method of Revil et al. (1999a). This potential decays exponentially throughout the thickness of the EDL on a scale that is characterized by the Debye length χ_D. The ζ can be obtained by considering the value of the electrical potential at the shear plane χ_ζ, which is an important input parameter to the model, and then adding the ζ offset (Glover et al. 2012a, b).

The zeta potential offset is a parameter that was introduced by Glover and Déry (2010) in the initial formulation of the model because it was recognized that the zeta potential calculated using the Revil et al. (1999a) approach did not provide values which matched the measured values at high salinities.

In this work, modelling has been carried out while setting the zeta potential offset ζ_0 to zero but it was not possible to find solutions of the overall model that would fit the measured zeta potential and streaming potential coefficient curves while retaining physically reasonable values of the other model parameters. Consequently, and in agreement with previous reports, it is concluded that a nonzero zeta potential offset is necessary for the operation of the model. The requirement for the zeta potential offset is probably due to a physical limit on the Debye length at high salinities caused by the size of the hydrated ions (Fig. 2f) (Vinogradov and Jackson 2015) or capacitor-like behaviour between excess

ions on the Stern plane and the shear plane if the latter is inside the Stern layer as proposed by Eq. (1) of Leroy et al. (2022).

Consequently, the results given in this paper arise from used of the model with $\zeta_0 = -9.5$ mV, kept constant irrespective of salinity or temperature. This assumption is forced by the lack of data allowing a more nuanced approach. In reality, it is likely that the zeta potential offset is both a function of temperature and salinity if we are correct in attributing it to a physical limit on the Debye length.

In the case of low and medium salinities the zeta potential is always much greater than the zeta potential offset, and the zeta potential offset will consequently have a small if not negligible effect on the final results. For high salinities, the zeta potential offset is needed for the model to provide physically realistic results, whether they match measurements or not. We implemented the model with a variable zeta potential offset such that at any salinity the total zeta potential was constrained to be greater than −9.5 mV, and found that the results were negligibly different from those presented in this paper.

This paper shows that the zeta potential generally decreases as temperature increases. Consequently, there will be a temperature where a zeta potential offset needs to be imposed if a physical limit needs to be introduced. This value is likely to be the same as that for salinity of it is caused by a physical limit.

The C_{sp} is calculated using one of the modified forms of the Helmholtz-Smoluchowski relationship (*e.g.*, Glover 2015) that were developed by Glover and Déry (2010). This model takes account of the individual microstructural parameters which describe the pore network (grain size d_{grain}, porosity ϕ, cementation exponent m, and formation factor F), allowing modelling to be carried out for individual samples. In this study I have carried out C_{sp} modelling for individual samples using d_{grain}, ϕ, m data given in Vinogradov and Jackson (2015). However, since their data is restricted to the two relatively high salinities, 0.01 mol/dm^3 and 0.5 mol/dm^3, the effect if the microstructure of the pores upon the streaming potential is smaller than it would be for samples saturated with lower salinity pore fluids. This allows a single curve to represent all 4 samples. I have used the data from the St. Bees 1 sandstone to calculate the curve, with the data shown in Table 1.

Other input parameters such as the pore fluid relative permittivity, viscosity and electrical conductivity, which were discussed earlier, are also temperature and salinity dependent. The final input parameter is the surface conduction. The surface conduction is made up of three contributions, each of which is calculated in the model using the methods in Revil and Glover (1997; 1998) and Revil et al. (1999a), and summed to provide an input to the final calculation, which is also temperature-dependent because it depends on a number of temperature-dependent parameters including pH. Unfortunately, there is no space to examine the temperature dependency of the surface conduction in this paper.

The sources and values of all the parameters used in the modelling are shown in Table 1. A full description of all the parameters used in the model together with independent measurements and the ranges over which they vary is given in Glover et al. (2012a, b) and in the supplementary material (Glover 2026).

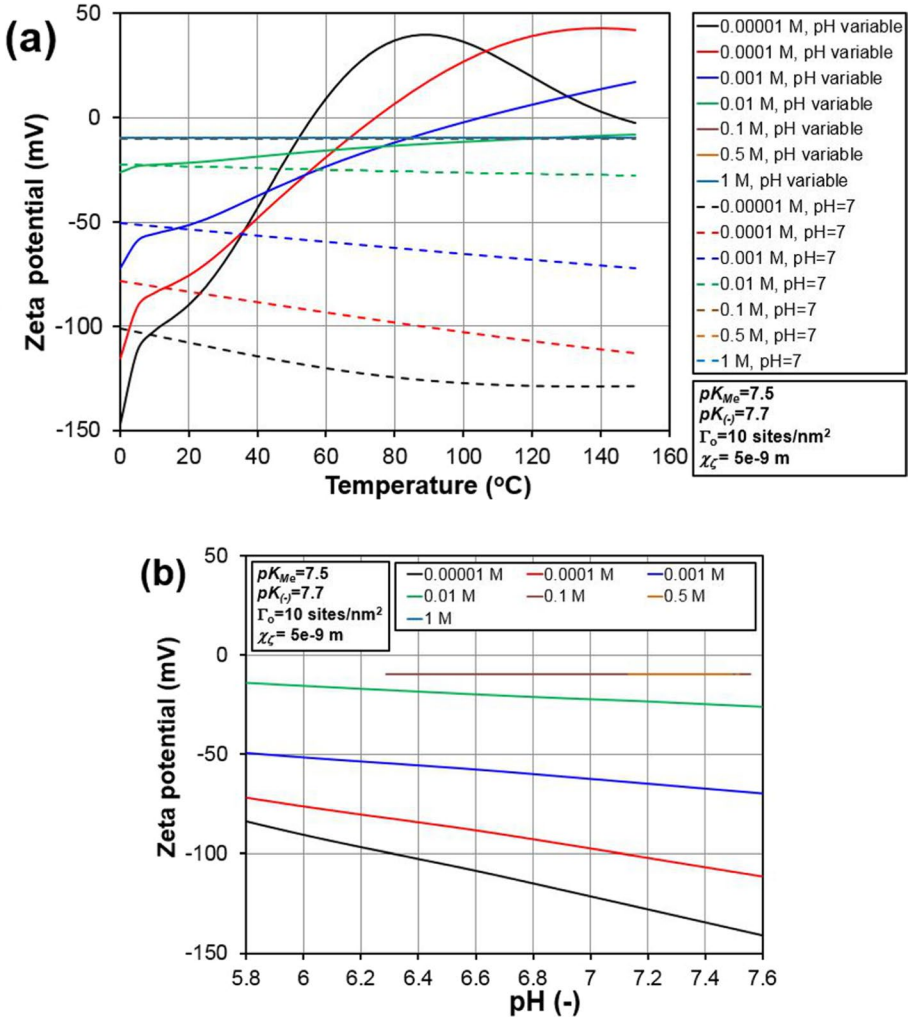

Fig. 3 The results of the model for the parameters shown in Table 1. **a** the ζ as a function of temperature with variable pH (solid lines) and fixed pH = 7 (dashed lines), **b** ζ as a function of pH (note the curves for 1, 0.5 and 0.1 mol/dm^3 are coincident), **c** C_{sp} as a function of temperature with variable *pH* (solid lines) and fixed pH = 7 (dashed lines), and **d** C_{sp} as a function of pH. Part **e** shows the same data as (**c**) but on linear axes in order to portray the full variation of the streaming potential without the curves being curtailed

5 Results

Figure 3 shows the implementation of the model for the calculation of ζ and C_{sp} as a function of temperature from 0 to 150°C and the consequential changes in pH for seven salinities from 10^{-5} to 1 mol/dm^3 and for the modelling parameters given in Table 1.

The ζ is negative at lower temperatures with larger magnitudes for lower salinities (Fig. 3a). As temperature increases, ζ decreases in magnitude at a faster rate for low salinity fluids than with higher salinity fluids ultimately becoming positive. This behaviour is

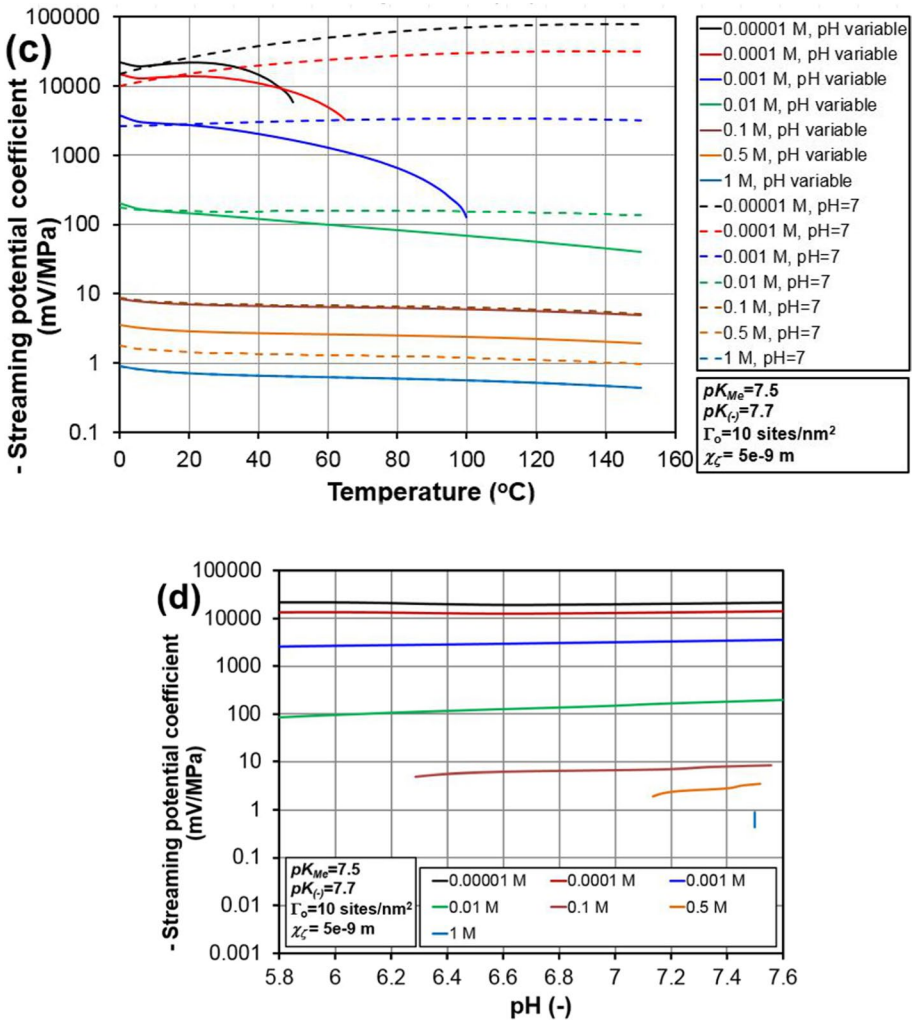

Fig. 3 (continued)

strongly influenced by the decrease in pH with temperature and its larger effect for low salinity solutions (see Fig. 2e). Comparison of the solid curves for variable pH with the dashed curves, which are calculated for a fixed pH = 7, shows the degree to which ζ is highly influenced by changing pH, which is supported by Fig. 3b showing the variation of ζ with pH. This agrees in all respects with the observations of Vinogradov and Jackson (2015). In each case the change is not linear, having a shape that is clearly influenced by the nonlinearity in the pH/temperature curve (Fig. 2e). The change in ζ over the temperature interval 0°C to 150°C varies with salinity, being −98.1% at 10^{-5} mol/dm^3, reaching the greatest change of −136.4% at 0.01 M and tending to zero change for salinities greater than 1 mol/dm^3 for the modelling parameters in Table 1. This is also consistent with the experimental measurements.

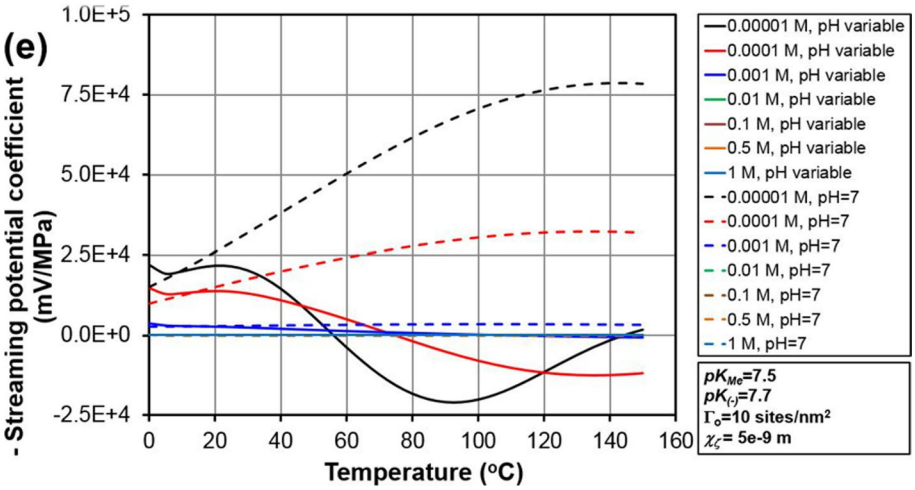

Fig. 3 (continued)

Varying the modelling parameters such as pK_{Me}, $pK_{(-)}$, Γ_0, and χ_ζ all change the sensitivity of the ζ to temperature, but the general pattern, with the greatest changes occurring for salinities between 0.001 mol/dm^{3}and 0.01 mol/dm^3, and with a tendency to negligible temperature dependence at high salinities, is retained. There is a greater sensitivity to temperature as pK_{Me}, $pK_{(-)}$ and Γ_0 all increase, though the effect is weak for pK_{Me}, and varying χ_ζ controls the salinity at which the greatest decrease of ζ per change in temperature occurs.

The behaviour of the C_{sp} is more complex as shown by Fig. 3c, e. These two parts show the same data but on differently scaled axes. Figure 3c uses a logarithmic axis which represents the large range of variation but curtails the curves when they become positive for the low salinity fluids, while Fig. 3e uses a linear scale which shows the full variation of the low salinity curves, but does not discriminate the high salinity curves whose small values become indistinguishable from zero when plotted this way.

Once again C_{sp} is always negative at low temperatures with much larger magnitudes for lower salinities. However, while C_{sp} increases slightly in magnitude as temperature increases for low salinities until about 20°C, it then decreases in magnitude significantly especially for the low salinity fluids. For the lowest salinities, it may be seen that the trend to become more positive stops after about 100°C, with the value of C_{sp} approaching zero as 1 mol/dm^3 is approached. These effects can be seen to be controlled by the behaviour of ζ, which is ultimately controlled by the pH variation. For medium to higher salinity fluids C_{sp} decreases in magnitude as temperature increases to 150°C remaining negative. The pH variation is also complex, decreasing with pH for low salinity pore fluids and increasing with pH for medium to high salinity pore fluids. Once again Fig. 3d and comparison of the solid curves for variable pH with the dashed curves for a fixed pH = 7 in Fig. 3c, e show the large influence of pH, approaching a factor of 10^4 in the case of 10^{-5} mol/dm^3 at 150°C. This behaviour also agrees well with the limited data coverage provided by Vinogradov and Jackson (2015).

The temperature dependence in C_{sp} over the temperature interval 0–150 °C varies with salinity, being −92.3% at 10^{-5} mol/dm^3, reaching the greatest negative change of −181.1%

at about 10^{-4} mol/dm^3, and tending towards a temperature dependence of about −52% for salinities greater than 1 mol/dm^3.

Once again, varying pK_{Me}, $pK_{(-)}$, Γ_0, and χ_ζ all change sensitivity of the ζ to temperature, but the general pattern, with the greatest positive temperature dependence occurring for the lowest salinities and the greatest negative temperature dependence between 0.001 mol/dm^3 and 0.01 mol/dm^3 with a tendency to negligible temperature dependence at high salinities, is retained. There is a greater sensitivity to temperature as pK_{Me}, $pK_{(-)}$ and Γ_0 all increase, especially at low salinities, though the effect is weak for pK_{Me}. Once again, varying χ_ζ controls the salinity at which the greatest decrease of ζ per change in temperature occurs, and increasing the protonic surface conduction (and hence the total surface conduction) only affects the C_{sp}, making the positive temperature dependence greater at low salinities and the negative temperature dependence weaker at high salinities.

Vinogradov and Jackson (2015) speculated that most of the temperature sensitivity of ζ was due to consequential changes in the pH of the pore solution, implementing a simplified model of the ζ for both variable and fixed mol/dm^3. This modelling confirms that such a hypothesis is consistent with the latest understanding, but shows that modelling with a fixed pH is invalid. Indeed, Fig. 3 also shows our modelling with a fixed pH = 7 (dashed lines), which is clearly in agreement with the limited ζ modelling at pH = 7 carried out by Vinogradov and Jackson (2015), and shows how the modelling results of both ζ and C_{sp} must include variable pH for pore fluids less than about 0.01 mol/dm^3.

We note particularly that the zeta potential becomes positive as temperature increases above about 82°C, 77°C and 52°C for 10^{-3} mol/dm^3, 10^{-4} mol/dm^3, and 10^{-5} mol/dm^3, respectively (Fig. 3a) and has a corresponding effect on the streaming potential coefficient (Fig. 3e). The model seems to be consistent with all of the data presented in Vinogradov and Jackson (2015). We know of no data for the higher temperature behaviour of sufficiently low salinity fluids, so cannot validate this behaviour, but note that it may not be realistic and may indicate that an important aspect of the model is lacking for low salinity fluids.

6 Case Study: The Vinogradov and Jackson (2015) data

While the previous section considered the general modelling results as a function of temperature, pH and salinity, this section considers how well the full model can fit the data provided by Vinogradov and Jackson (2015). The large number of parameters in the model implies that a good fit might be possible. However, detailed examination reveals that many of these parameters are fixed by the conditions of the experiment or independent measurements, and where there is scope for varying the parameters, independent electro-chemical measurements restrict the range over which the remainder may be varied. Consequently, of the 22 input parameters listed in Table 1, 8 of them are defined by the temperature and pressure conditions of the measurements (T, C_f and the 6 empirical relationships), 4 of them are rock-specific parameters or other parameters provided by Vinogradov and Jackson (2015) (ϕ, m, d_{grain} and ζ_0), 7 are electro-chemical parameters for which the values are well-known or to which the model is relatively insensitive (pK_{Me}, Σ_s^{prot}, β_s, β_{Na^+}, β_{H^+}, β_{Cl^-}, β_{OH^-}) leaving three parameters ($pK_{(-)}$, Γ_0, and χ_ζ)which exert the greatest control over the shape of the ζ and C_{sp} curves. These three parameters

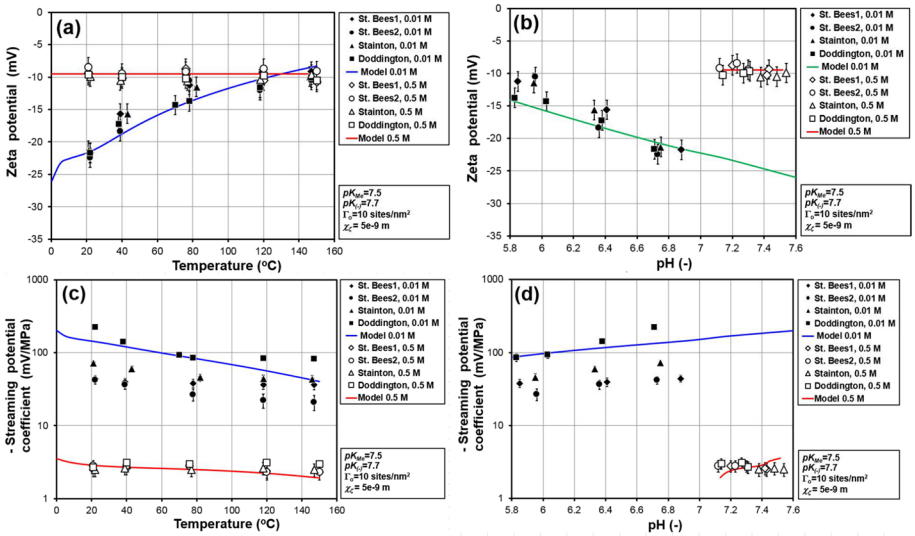

Fig. 4 Implementation of the model for the parameters pertaining to the data from Vinogradov and Jackson (2015). **a** the ζ as a function of temperature, **b** ζ as a function of pH, **c** C_{sp} as a function of temperature, and **d** C_{sp} as a function of pH. Modelling parameters are shown in Table 1

are constrained by independent measurements to specific ranges ($6.5 < pK_{(-)} < 8.5$; $2.6 < \Gamma_0 < 25$; 2×10^{-10} m $< \chi_\zeta < 5 \times 10^{-10}$ m), which are sourced and discussed in full in Sect. 3 above and in Glover et al. (2012a, b).

The modelling values used in this study (Table 1) provide the closest fit of the ζ and C_{sp} curves to the data while varying these three parameters within the experimental ranges. The fit was carried out by manual exploration rather than any curve fitting process and consequently a slightly better fit might be obtained by using slightly different input parameter values.

Figure 4 shows the results of modelling the Vinogradov and Jackson (2015) ζ and C_{sp} data as a function of temperature and pH for both of the experimental salinities. The models perform creditably in all cases but cannot be considered to be an exact match to the data. This is likely to be due to a combination of experimental errors and inadequacies in the model.

For the ζ the high salinity data (0.5 mol/dm^3) as a function of both temperature and pH is modelled well mainly because its value is controlled by the imposed value of the ζ offset (−9.5 mV).

The model for the lower salinity (0.01 mol/dm^3) as a function of pH is also modelled very well, while that as a function of temperature reproduces the sign, approximate magnitude and shape of the data well, but overestimate the magnitude in the middle salinities by about 3 mV, which I regard as a creditable performance.

The fit to the temperature dependence can be improved by small changes to the three main parameters (*e.g.*, any one of $pK_{(-)}$ 7.7 → 8.0; Γ_0 10 → 7; χ_ζ 3.5×10^{-9}), all of which remain within the acceptable range, but λin each case the fit to the pH dependency is degraded for temperatures above 150°C. The reason for this small difference in the model efficacy is not easy to ascertain. It might be that there was a systematic error in either the temperature or pH measurement, but this is very unlikely as an error of

either 30°C, or 0.3 pH points would be necessary. Another reason could be a failure of the relationship between temperature and pH used in the model, but this is a well-known and well-tested empirical relationship. A third, and more plausible reason might be that the pH in the rock is different from that calculated in the model because of reactions between the pore fluid and the rock matrix. It was recognized (Revil and Glover 1997) that the pore fluid pH changes within the EDL, and that there is some uncertainty as to the value of pH that ought to be used in the modelling of process operating at these scales, and which define the ζ and C_{sp}.

For the C_{sp} modelling of both the high salinity data (0.5 mol/dm^3) and the lower salinity (0.01 mol/dm^3) as a function of both temperature and pH reproduces the sign, approximate magnitude and trend of the data well, with the model underestimating the high salinity data by a factor of 2 and falling within the spread of the low salinity data.

It is tempting to ascribe the spread of the C_{sp} data to variations in the pore microstructure between the samples measured by Vinogradov and Jackson (2015), which includes samples with porosities ranging from 0.13 to 0.19, cementation exponents ranging from 1.34 to 1.86, formation factors between 10 and 45 and grain sizes from 60×10^{-5} m to 200×10^{-5} m. Analysis of the magnitudes of the C_{sp} measurements shows no obvious relationship to the microstructural parameters. In any case, the microstructural parameters have almost no effect on the modelled C_{sp}, for these high salinities. The curves shown in Fig. 4 are for St. Bees1 parameters. Implementation of the model for any of the other of the Vinogradov and Jackson (2015) rocks moves the curve by a very small amount, insufficient to allow the curve to match the relevant data points.

7 Conclusions

Vinogradov and Jackson (2015) have reported experimental measurements of C_{sp} and derived ζ. The Glover et al. (2012a, b) approach for calculating the ζ and C_{sp} or porous silica-based rocks filled with aqueous NaCl pore fluids has been implemented as a function of temperature, pH and salinity. The model curves reproduce the sign, magnitude and shape of the ζ and C_{sp} as a function of both temperature and pH dependence, fitting the Vinogradov and Jackson (2015) data reasonably well. However, small discrepancies between the model and the data show that there is scope for improvement of the model, and new experimental methodologies (Walker et al. 2014).

The modelling confirms Vinogradov and Jackson's (2015) assertion that the temperature effect on both the ζ and the C_{sp} is mainly through its effect on the pH of the pore fluid. While the temperature dependencies of the ζ and the C_{sp} have long been ambiguous, the combination of the Vinogradov and Jackson (2015) data with the modelling carried out in this work has confirmed the sign, magnitude and trend of these parameters as temperature, pH and salinity varies, opening the door for more accurate electro-kinetic predictions in hydrocarbon exploration and production, geothermal resources, aquifers, prospective sites for carbon capture and storage by deep underground injection, and in characterising subsurface sites for the storage of radioactive waste.

I have been made aware of further datasets that might be treated by this model (Hidayat et al. 2022; Vinogradov 2024). While such data cannot be included in this paper due to time constraints, this modelling will be prepared for a further publication.

Supplementary Information The online version contains supplementary material available at https://doi.org/10.1007/s11242-026-02321-5.

Acknowledgements The author would like to thank 3 anonymous reviewers for their detailed reading, support and constructive comments that have much improved the paper.

Author Contributions P.W.J.G. is the sole researcher and author of this work.

Funding This work received no funding

Data Availability Full supplementary information is available at (Glover P. (2026). Modified theoretical model for temperature-dependent electro-kinetic properties of porous media—Supplementary material—Model. In Zenodo. https://doi.org/10.5281/zenodo.19133221). This information includes the model implemented in Excel with active graphics, and (ii) a large summary diagram which shows the main functional associations within the model.

Declarations

Conflict of interest The authors declare no conflicts of interest relevant to this study.

References

Alekhin, Y.V., Sidorova, M.P., Ivanova, L.I., Lakshtanov, L.Z.: Investigation of the electrokinetic potential and adsorption of ions on Al_2O_3 and SiO_2 at high temperature and pressures. Kolloidn. Zh. **46**, 1195–1198 (1984)

Bernabé, Y., Mok, U., Maineult, A., Evans, B.: Laboratory measurements of electrical potential in rock during high-temperature water flow and chemical reactions. Geothermics **32**(3), 297–310 (2003). https://doi.org/10.1016/S0375-6505(03)00020-8

Booth, F.: The dielectric constant of water and the saturation effect. J. Chem. Phys. **19**, 391–394 (1951). https://doi.org/10.1063/1.1748233

Crow, D.R.: Principles and Applications of Electrochemistry. Chapman and Hall, London (1988)

Dove, P.M., and J.D. Rimstidt: Silica-Water Interactions: in Reviews in Mineralogical Series: The Silica Polymorphs, edited by P.J. Heaney, C.T. Prewitt, and G.V. Gibbs, 30, 210–260, Mineral. Soc. Am., Washington, D.C (1994)

Dunstan, D.E.: Temperature-dependence of the electrokinetic properties of two disparate surfaces. J. Colloid Interface Sci. **166**, 472–475 (1994). https://doi.org/10.1006/jcis.1994.1319

Dupuis, J., Butler, K., Kepic, A., Harris, B.: Anatomy of a seismoelectric conversion: measurements and conceptual modeling in boreholes penetrating a sandy aquifer. J. Geophys. Res. (2009). https://doi.org/10.1029/2008JB005939

Glover, P.W.J.: Modelling pH-dependent and microstructure-dependent streaming potential coefficient and zeta potential of porous sandstones. Transp. Porous Med. **124**, 31–56 (2018). https://doi.org/10.1007/s11242-018-1036-z

Glover, P.W.J., Déry, N.: Dependence of streaming potential on grain diameter and pore radius for quartz glass beads. Geophysics **75**(6), F225-241 (2010). https://doi.org/10.1190/1.3509465

Glover, P.W.J., Walker, E., Jackson, M.D.: Streaming-potential coefficient of reservoir rock. Geophysics **77**(2), D17–D43 (2012a). https://doi.org/10.1190/GEO2011-0364.1

Glover, P.W.J., Walker, E., Ruel, J., Tardif, E.: Frequency-dependent streaming potential of porous media—Part 2: experimental measurement of unconsolidated materials. Int. J. Geophys. **2012**, 728495 (2012b). https://doi.org/10.1155/2012/728495

Glover, P.W.J., Peng, R., Lorinczi, P., et al.: Experimental measurement of frequency-dependent permeability and streaming potential of sandstones. Transp. Porous Media **131**, 333–361 (2020). https://doi.org/10.1007/s11242-019-01344-5

Glover, P.W.J.: Geophysical Properties of the Near Surface Earth: Electrical Properties. In: Gerald Schubert (editor-in-chief) Treatise on Geophysics, 2nd edition, Vol 11,p. 89–137. Oxford: Elsevier (2015)

Glover, P.:Modified theoretical model for temperature-dependent electro-kinetic properties of porous media - Supplementary material - Model. In Not yet published (1.1). Zenodo. https://doi.org/10.5281/zenodo.19133221 (2026)

Grahame, D.C.: Effects of dielectric saturation upon the diffuse double layer and free energy of hydration of ions. J. Chem. Phys. **18**, 903–909 (1950)

Hidayat, M., Sarmadivaleh, M., Derksen, J.J., Vega-Maza, D., Iglauer, S., Vinogradov, J.: Zeta potential of CO_2-rich aqueous solutions in contact with intact sandstone sample at temperatures of 23 °C and 40 °C and pressures up to 10.0 MPa. J. Colloid Interface Sci. **607**, 1226–1238 (2022). https://doi.org/10.1016/j.jcis.2021.09.076

Hiemstra, T., Van Riemsdijk, W.H.: Multiple activated complex dissolution of metal (hydr) oxides: a thermodynamic approach applied to quartz. J. Colloid Interface Sci. **136**, 132–150 (1990). https://doi.org/10.1016/0021-9797(90)90084-2

Hunter, R.J.: The interpretation of electrokinetic potentials. J. Colloid Interface Sci. **22**, 231–239 (1966). https://doi.org/10.1016/0021-9797(66)90028-2

Hunter, R.J.: Zeta Potential in Colloid Science. Academic Press, New York (1981)

Iglesias, T.P., Péon Fernandez, J.: A mixing rule for the permittivity of binary mixtures in a framework of a weak-fluctuations model. J. Mater. Sci. Lett. **20**, 1333–1324 (2001). https://doi.org/10.1023/A:1010962920679

Iler, R.K.: The Chemistry of Silica. Wiley, New York (1979)

Ishido, T., Mizutani, H.: Experimental and theoretical basis of electro-kinetic phenomena in rock-water systems and its applications to geophysics. J. Geophys. Res. **86**(B3), 1763–1775 (1981). https://doi.org/10.1029/JB086iB03p01763

Jaafar, M.Z., Vinogradov, J., Jackson, M.D.: Measurement of streaming potential coupling coefficient in sandstones saturated with high salinity NaCl brine. Geophys. Res. Lett. **36**, L21306 (2009). https://doi.org/10.1029/2009GL040549

Jaafar, M.Z.: Measurement of Streaming Potential for Oilfield Monitoring in Intelligent Wells: PhD Thesis, Imperial College London, UK (2009)

Johnson, D.L., Koplik, J., Dashen, R.: Theory of dynamic permeability in fluid saturated porous media: J. Fluid. Mech., 176, 379–402.Jørgensen, S.S., and A.T. Jensen, 1967, Acid-base properties of quartz suspensions. J. Phys. Chem. **71**, 745–750 (1987). https://doi.org/10.1021/j100862a040

Jørgensen, S.S., Jensen, A.T.: Acid-base properties of quartz sus-pensions. J. Phys. Chem. **71**, 745–750 (1967). https://doi.org/10.1021/j100862a040

Kell, G.S.: Density, thermal expansivity, and compressibility of liquid water from 0° to 150°C: Correlations and tables for atmospheric pressure and saturation reviewed and expressed on the 1968 temperature scale. J. Chem. Eng. Data **20**(1), 97–105 (1975). https://doi.org/10.1021/je60064a005

Kosmulski, M.: Adsorption of cadmium on alumina and silica: analysis of the values of stability constants of surface complexes calculated for different parameters of triple layer model. Colloids Surf. A Physicochem. Eng. Aspects **117**, 201–214 (1996)

Leroy, P., Maineult, A., Li, S., Vinogradov, J.: The zeta potential of quartz: surface complexation modelling to elucidate high salinity measurements. Colloids Surf A Physicochem Eng Asp **650**, 129507 (2022). https://doi.org/10.1016/j.colsurfa.2022.129507

Lide, D.R.: Handbook Of Chemistry And Physics, 90th ed.: CRC Press (200)

Lorne, B., Perrier, F., Avouac, J.-P.: Streaming potential measurements 1. properties of the electrical double layer from crushed rock samples. J. Geophys. Res. **104**, 17857–17877 (1999). https://doi.org/10.1029/1999JB900156

Lyklema, J., Overbeek, J.T.G.: On the interpretation of electrokinetic potentials. J. Colloid Interface Sci. **16**, 501–512 (1961). https://doi.org/10.1016/0095-8522(61)90029-0

Maineult, A., Bernabé, Y., Ackerer, P.: Electrical response of flow, diffusion, and advection in a laboratory sand box. Vadose Zone J. **3**, 1180–1192 (2004)

Morgan, F.D., Williams, E.R., Madden, T.R.: Streaming potential properties of Westerly Granite with applications. J. Geophys. Res. **94**, 12449–12461 (1989). https://doi.org/10.1029/JB094iB09p12449

Novotný, P., Söhnel, O.: Densities of aqueous solutions of inorganic substances: a comprehensive correlation. J. Chem. Eng. Data **33**(1), 49–55 (1988)

O'Konski, C.T.: Electric properties of macromolecules, V: theory of ionic polarization in polyelectrolytes. J. Chem. Phys. **64**, 605–619 (1960)

Overbeek, J.Th.G.: Electrochemistry of the double layer: Colloid Science 1, Irreversible Systems, edited by H.R. Kruyt, 115- 193, Elsevier, New York (1952)
Park, J., Regalbuto, J.R.: A simple, accurate determination of oxide PZC and the strong buffering effect of oxide surfaces at incipient wetness. J. Colloid Interface Sci. **175**, 239–252 (1995)
Phillips, S.L., H. Ozbek, and R.J. Otto: Basic energy properties of electrolytic solutions database: (1978) paper presented at Sixth International CO-DATA Conference, 2–25, accessed 10 June 2010, http://www.etde.org/etdeweb/purl.cover.jsp?purl=/6628103-xaRVpW/
Pride, S.R., Morgan, F.D.: Electrokinetic dissipation induced by seismic waves. Geophysics **56**, 914–925 (1991). https://doi.org/10.1190/1.1443125
Reppert, P., Morgan, F.: Temperature dependent streaming potentials: 1. theory. J. Geophys. Res. **108**, 2546 (2003a). https://doi.org/10.1029/2002JB001754
Reppert, P., Morgan, F.: Temperature dependent streaming potentials: 2. laboratory. J. Geophys. Res. **108**, 2547 (2003b). https://doi.org/10.1029/2002JB001755
Revil, A., Cathles, L.M.: Permeability of shaly sands. Water Resour. Res. **35**, 651–662 (1999). https://doi.org/10.1029/98WR02700
Revil, A., Glover, P.W.J.: Theory of ionic surface electrical conduction in porous media. Phys. Rev. B **55**(3), 1757–1773 (1997)
Revil, A., Glover, P.W.J.: Nature of surface electrical conductivity in natural sands, sandstones, and clays. Geophys. Res. Lett. **25**(5), 691–694 (1998)
Revil, A., Pezard, P.A., Glover, P.W.J.: Streaming potential in porous media: 1. theory of the zeta potential. J. Geophys. Res. **104**(B9), 20021–20031 (1999a). https://doi.org/10.1029/1999JB900089
Revil, A., Schwaeger, H., Cathless, L.M., Manhardt, P.D.: Streaming potential in porous media 2. theory and application to geothermal systems. J. Geophys. Res. **104**, 20033–20048 (1999b). https://doi.org/10.1029/1999JB900090
Rustad, J.R., Wasserman, E., Felmy, A.R., Wilke, C.: Molecular dynamics study of proton binding to silica surfaces. J. Colloid Interface Sci. **198**, 119–129 (1998)
Saunders, J., Jackson, M., Pain, C.: Fluid flow monitoring in oil fields using downhole measurements of electrokinetic potential. Geophysics **73**(5), E165–E180 (2008)
Saunders, J.H., Jackson, M.D., Gulamali, M.Y., Vinogradov, J., Pain, C.C.: Streaming potentials at hydrocarbon reservoir conditions. Geophysics **77**, E77–E90 (2012). https://doi.org/10.1190/geo2011-0068.1
Scales, P.J., Grieser, F., Healy, T.W.: Electrokinetics of the muscovite mica-aqueous interface. Langmuir **6**, 582–589 (1990)
Sen, P., Goode, P.: Influence of temperature on electrical conductivity on shaly sands. Geophysics **57**, 89–96 (1992a). https://doi.org/10.1190/1.1443191
Sen, P., Goode, P.: Errata, to "Influence of temperature on electrical conductivity of shaly sands." Geophysics **57**, 89 (1992b). https://doi.org/10.1190/1.1443191
Smith, A.L.: Electrokinetics of the oxide - solution interface. J. Colloid Interface Sci. **55**(3), 525–530 (1976). https://doi.org/10.1016/0021-9797(76)90062-X
Tadros, T.F., Lyklema, J.: The electrical double layer on silica in the presence of bivalent counter-ions. J. Electroanal. Chem. Interfacial Electrochem. **22**, 1–7 (1969)
Tardif, E., Glover, P.W.J., Ruel, J.: Frequency-dependent streaming potential of Ottawa sand. J. Geophys. Res. **116**, B04206 (2011). https://doi.org/10.1029/2010JB008053
Tardif, E., Glover, P.W.J., Ruel, J.: Frequency-dependent streaming potential of porous media—Part 1: experimental approaches and apparatus design. Int. J. Geophys. (2012). https://doi.org/10.1155/2012/846204
Vinogradov, J., Jackson, M.D.: Zeta potential in intact natural sandstones at elevated temperatures. Geophys. Res. Lett. **42**(15), 6287–6294 (2015). https://doi.org/10.1002/2015GL064795
Vinogradov, J., Hidayat, M., Sarmadivaleh, M., Vega-Maza, D., Iglauer, S., Zhang, L., Mei, D., Derksen, J.: Zeta potential of supercritical CO_2-water-sandstone systems and its correlation with wettability and residual subsurface trapping of CO_2. Water Resour. Res. **60**(11), e2023WR036698 (2024). https://doi.org/10.1029/2023WR036698
Walker, E., Glover, P.W.J.: Permeability models of porous media: characteristic length scales, scaling constants and time-dependent electrokinetic coupling. Geophysics **75**(6), E235–E246 (2010). https://doi.org/10.1190/1.3506561
Walker, E., Glover, P.W.J.: Measurements of the relationship between microstructure, pH, and the streaming and zeta potentials of sandstones. Transp. Porous Media **121**, 183–206 (2018). https://doi.org/10.1007/s11242-017-0954-5

Walker, E., Glover, P.W.J., Ruel, J.: A transient method for measuring the DC streaming potential coefficient of porous and fractured rocks. J. Geophys. Res. Solid Earth **119**(2), 957–970 (2014). https://doi.org/10.1002/2013JB010579

Watillon, A., de Backer, R.: Potentiel d'écoulement, courant d'écoulement et conductance de surface à l'interface eau-verre. J. Electroanal. Chem. **25**, 181–196 (1970). https://doi.org/10.1016/S0022-0728(70)80336-9

Waxman, M.H., Smits, L.J.M.: Electrical conductivities in oil-bearing shaly sands. Soc. Pet. Eng. J. **8**, 107–122 (1968)

Wu, L., Forsling, W., Schlindler, P.W.: Surface complexation of calcium minerals in aqueous solution. J. Colloid Interface Sci. **147**, 178–185 (1991)

Yates, D.E., Healy, T.W.: The structure of the silica/electrolyte interface. J. Colloid Interface Sci. **55**, 9–19 (1976)